NATIONAL AERONAUTICS AND SPACE ADMINISTRATION

Technical Report No. 32-923

Effect of Predeformation on the Mechanical Properties of Sodium Chloride Crystals

P. J. Shlichta

JET PROPULSION LABORATORY
CALIFORNIA INSTITUTE OF TECHNOLOGY
PASADENA, CALIFORNIA

May 1, 1966

NATIONAL AERONAUTICS AND SPACE ADMINISTRATION

Technical Report No. 32-923

Effect of Predeformation on the Mechanical Properties of Sodium Chloride Crystals

P. J. Shlichta

C. E. Lesse, Manager
Materials Section

JET PROPULSION LABORATORY
CALIFORNIA INSTITUTE OF TECHNOLOGY
PASADENA, CALIFORNIA

May 1, 1966

Prepared Under Contract No. NAS 7-100
National Aeronautics & Space Administration

CONTENTS

TABLES

FIGURES

ABSTRACT

Sodium chloride crystals were grown from melt as uniform <100> rods, 3 to 5 mm in diam with flat {100} faces. The mechanical properties of these as-grown crystals were compared with those of predeformed crystals and with annealed, water-polished cleavages of comparable size, purity, and dislocation density. Bend tests were performed using four-point loading at strain rates of 1.5 to 3 $\times$ 10^{-5}/sec. The load and deflection data were reduced, under the assumption of quasi-elastic behavior, to obtain T, the outer-fiber {110} <1$\bar{1}$0> shear stress and E, the outer-fiber tensile strain.

The stress-strain curves of the as-grown crystals were similar to those of face-centered cubic metals; they showed a sharp yield point, a region of easy glide of slope $G_I = \overline{dT/dE}$, and a second stage of increased work-hardening rate beginning at 5.5 to 8% strain. A linear relation existed between G_I, the yield stress (T_y), and the calcium concentration (C):

$$G_I \simeq 33.5\,(T_y - 18) \simeq 184C$$

This suggests that a pure, as-grown crystal would have a yield stress of 18 g/mm^2 and virtually no work hardening during the first stage of deformation.

In contrast, the stress-strain curves of the predeformed crystals and cleavages showed numerous idiosyncrasies, such as anelastic feet and soft vs stiff behavior. Moreover, the G_I of these specimens was invariably higher than that predicted for as-grown crystals of comparable yield stress. These idiosyncrasies are, therefore, attributed to artifacts (e.g., slip bands) introduced during cleavage or predeformation. The soft vs stiff effect is attributed to the orientation of the predeformation slip systems with respect to those activated during the test; the effect is, therefore, related to the phenomenon of latent hardening, which apparently persists through annealing.

Although the as-grown crystals were exposed to divers atmospheric environments prior to testing, there was no indication of embrittlement. This suggests that the embrittlement of cleavages is due to the interaction of emerging slip bands with the atmosphere. The only

ABSTRACT (Cont'd)

effect of water polishing was to increase the rate of stage II work hardening. When bent under water, however, the as-grown crystals showed a dramatic increase in ductility and could be tied in knots. This increase in ductility cannot be accounted for by most of the current explanations of the Joffe effect; therefore, it is proposed that this dynamic Joffe effect is a consequence of the enhanced solubility of stressed crystal surfaces.

It is concluded that most of the inconsistencies in the existing literature on the mechanical properties of sodium chloride crystals are the result of artifacts introduced during cleavage or polishing. Therefore, only as-grown crystals, of the highest possible purity and perfection, should be used in future research on the subject.

I. INTRODUCTION

Sodium chloride crystals sometimes exhibit a high degree of ductility, in many respects comparable to that of face-centered cubic metals (Ref. 1). In general, the mechanical properties depend drastically on the prior history of the crystals; moreover, there is a wide range of idiosyncrasies among specimens with identical histories. These idiosyncrasies are summarized in the following paragraphs.

An anelastic region of initial deformation, prior to the elastic region, is often observed. This "foot" on the stress-strain curve is sensitive to the pretreatment given the specimen and is attributed to dislocation loops introduced into the specimen by cleavage (Ref. 2).

The yield stress and the shape of the stress-strain curve vary erratically from one specimen to another. This variation appears to depend on such aspects of the history of the specimen as the annealing temperature, time, and cooling rate (Refs. 2 and 3), exposure to atmosphere during and after annealing (Refs. 3 and 4), water polishing of the surfaces (Ref. 2), and impurity content (Ref. 3).

Bend tests of specimens cleaved or sawed from a single crystal block show two distinct classes of behavior: (1) "soft", low rate of work-hardening; and (2) "stiff", high rate of work-hardening (Refs. 5 and 6). Crystals showing one type of deformation exhibit the other when rotated 90 deg with reference to the axis of bending. In unannealed water-polished cleavages, the type of deformation can be predicted from the pre-existing slip systems (i.e., the birefringence patterns); therefore, the effect is attributed to strain introduced during cleavage. There appears to be no such correlation, however, for annealed specimens (Ref. 6).

The overall ductility of sodium chloride crystals is greatly affected by surface treatment. Abrasion or scratching causes drastic embrittlement (Ref. 5). Freshly cleaved specimens exhibit considerable ductility but

rapidly become brittle when exposed to the atmosphere. Water polishing of the cleavage surfaces restores and even enhances the original ductility (Ref. 7); subsequent exposure to the atmosphere may or may not cause re-embrittlement. These effects have been attributed to reaction with oxygen or nitrogen (Ref. 8), the formation of $NaClO_3$ surface barrier (Ref. 9), the reaction of CO_2 with OH ions on the crystal surface (Ref. 10), or to the presence of stress-concentrating steps caused either by dissolution and recrystallization in moist air (Ref. 11), or by the evaporation of residual polishing solution (Ref. 12).

It is important to note that all of the preceding observations were made on *cleavages* of sodium chloride crystals although, in this material, the process of cleaving always results in deformation throughout the entire crystal. Specimens observed between crossed polaroids invariably show slip bands (i.e., networks of birefringence bands). Frequently, when thin rods are cleaved for tension or bend tests, the specimens are visibly warped or curved. The customary starting material for this type of research—random pieces from optical-quality commercial crystals—invariably exhibit birefringence bands as received. Alden (Ref. 13) has demonstrated that activated slip systems in alkali halide crystals inhibit or hinder the operation of the other nonorthogonal slip systems; this phenomenon is known as latent hardening. Moreover, the process of cleavage causes extensive surface damage in the form of cracks, cleavage steps, dislocation loops (Ref. 14), and localized areas of extensive deformation. All of these defects, which can extend to a considerable depth below the cleavage surface, can greatly affect the mechanical properties of a specimen.

It may be therefore concluded that some, or all, of the idiosyncrasies in mechanical behavior of sodium chloride are the result of artifacts introduced during cleavage. Accordingly, the proper material for study would be as-grown crystals, free from all predeformation and surface damage. The work described in this Report represents a preliminary survey to determine whether macroscopic as-grown crystal rods of sodium chloride show more uniform, reproducible, and comprehensible mechanical properties than annealed, water-polished cleavages of the type usually studied.

II. EXPERIMENTAL

A. Crystal Rods

A study (Ref. 15) of the morphology of NaCl crystals, pulled from melt by the Kyropoulos-Czochralski method, disclosed two modes of growth for crystals grown in the <100> direction: (1) a rounded, ridged form, favored by high melt temperatures, slow pull rates, or decreasing cross section; and (2) a faceted form, with well developed {100} faces, favored by low melt temperatures, fast pull rates, or increasing cross section. Mode (2) is presumably a nonequilibrium form, controlled by the absence of growth-step forming nuclei. By careful control of temperature, pull rate, and seeding procedure, it was possible to grow thin uniform <100> rods with a rounded-square cross section and prominent {100} faces. The dominance of the {100} faces so stabilized the <100> orientation of the rods that, if the seed was inserted with the <100> direction at a 5- to 10-deg angle from the vertical, the crystal rod grew in the <100> rather than the vertical direction.

The crystal rods used for the tests were grown in the apparatus shown in Figs. 1 and 2. The furnace, containing conventional nichrome semicylindrical heating elements, was mounted in an aluminum dry box. The pull rod was introduced through an O-ring seal. An ungettered argon atmosphere was used; the system was evacuated to ~10 microns and flushed with argon two or more times. Reagent-grade sodium chloride was used, without

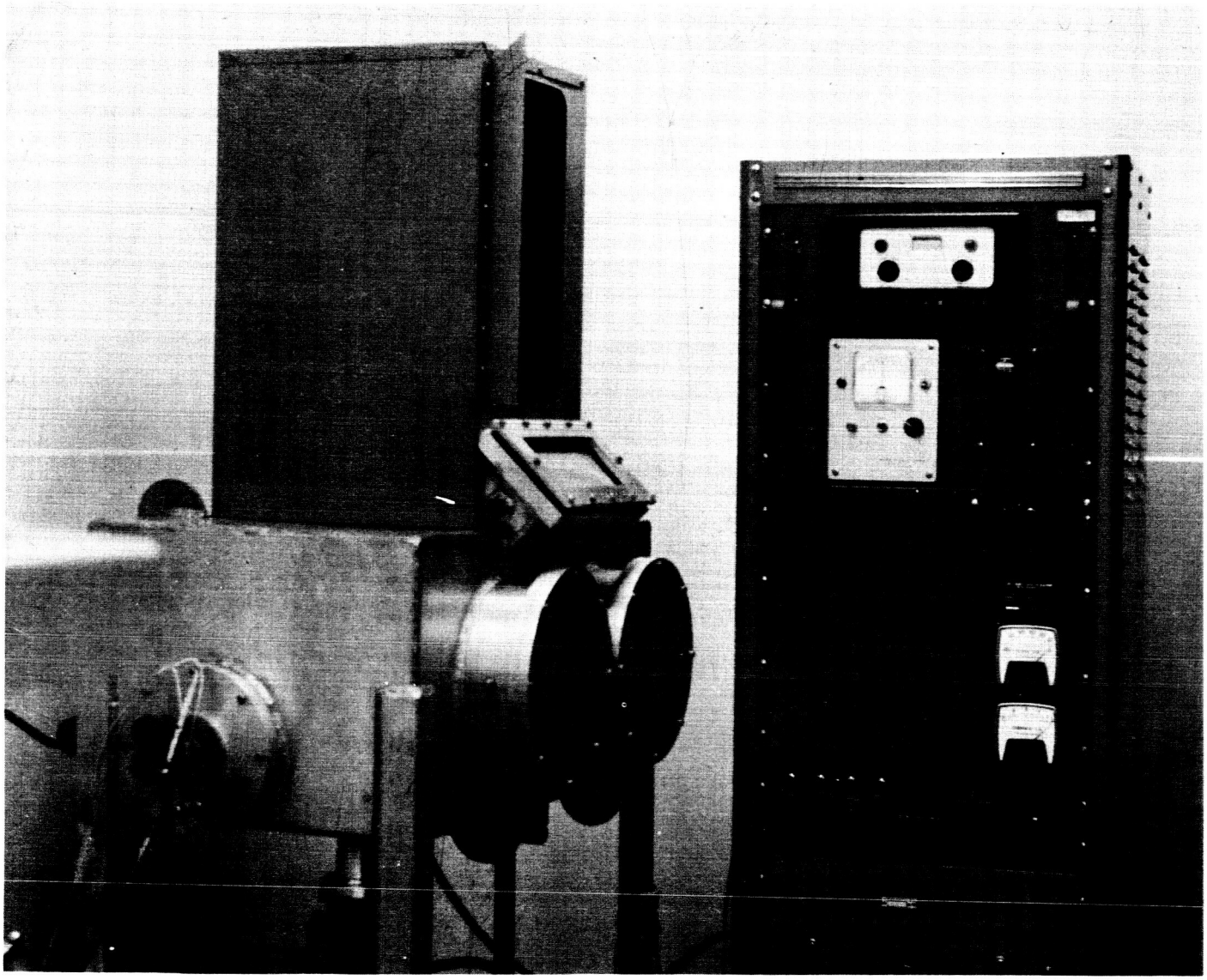

Fig. 1. Exterior view of crystal grower showing pull mechanism, vacuum pump, and view port

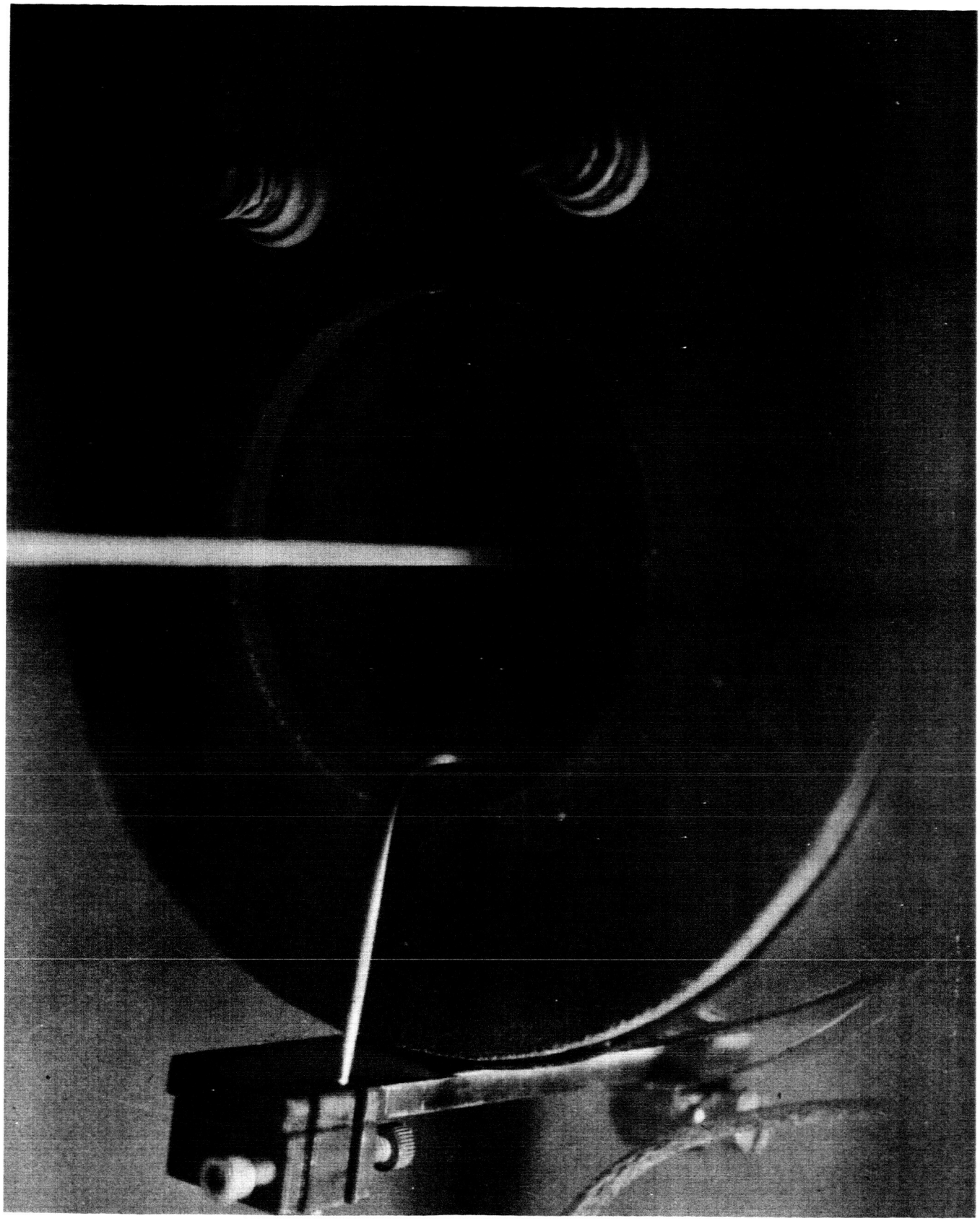

Fig. 2. Interior view of crystal grower, through view port, showing furnace and crystal rod during latter part of growth cycle

further purification, as the starting material (a typical analysis is shown at the bottom of Table 1). The salt was melted in nuclear-grade graphite crucibles. In summary, no attempt was made to produce crystals of unusually high purity.

A typical crystal rod is shown in Fig. 3. The {100} faces are typically half as wide as the diameter of the crystal (i.e., 3 to 4 mm) and are, within the limits of microscopic observation, flat and smooth, except for occasional growth steps presumably nucleated by dirt particles in the melt or by abrupt changes in temperature or pull rate. On a few of the crystals, one of the {100} faces is completely rounded, presumably because of a hot spot on the corresponding side of the furnace during growth. The edges are rounded and tend to undulate slightly, thereby reflecting slight variations in growth conditions. In those cases where the crystal was rotated during growth, the edges are slightly ridged. The crystals showed no trace of a birefringence pattern under crossed polaroids.

All of the crystals were stored for over a year before testing, sometimes in a dessicator, and sometimes in the open air under widely varying conditions of humidity and NO_2 or ozone concentrations. Thus, there would appear to have been ample opportunity for atmospheric embrittlement prior to testing; in fact, the crystal surfaces

Table 1. Spectrochemical analyses of NaCl cleavages, crystal rods, and starting material

Test specimen	Element							Other[a]
	Si	Mg	Cu	Ca	Al	Fe	Y	
	"Limits of detection"							[a]
	10 ppm	0.5 ppm	0.5 ppm	1 ppm	4 ppm	5 ppm	30 ppm	[a]
Cleavages								
1-1	—	—	1.1	20	—	—	—	Nil
5-1	29	—	1.5	14	—	—	—	
5-3	—	—	1.0	8.6	—	—	—	
6-2	Trace	—	1.7	8.4	—	—	—	
6-3	—	—	6.8	8.2	—	—	—	
14-2	—	—	0.8	12	—	—	—	
15-1	—	—	0.7	13	—	—	—	
22-1	—	—	1.3	10	—	—	—	
22-2	Trace	—	1.1	9.6	—	—	—	
25-1	46	—	1.8	21	—	Trace	—	
25-2	Trace	—	1.8	14	—	—	—	
25-3	Trace	—	1.5	15	—	—	—	
26-1	—	—	1.0	19	—	—	—	
26-2	—	—	0.8	7.4	—	—	—	Nil
As-grown crystals								
6-1	—	—	0.8	29	—	—	—	Nil
	27	—	1.2	24	—	—	—	
	39	—	1.1	16	—	—	—	
7-1	—	—	1.9	15	—	—	—	
	19	—	1.7	17	—	—	—	Nil
7-2	210	Trace	1.1	13	10	7	—	Nil
	26	—	1.8	9.5	—	—	—	
7-3	—	—	1.0	12	—	17	69	
7-4	—	—	1.2	11	—	7	—	
	89	—	1.9	11	15	63	—	
8-1	Trace	—	1.0	24	—	—	—	
	16	—	2.9	18	—	—	—	
8-3	—	—	1.5	25	—	—	—	Nil
Predeformed crystals								
8-2	Trace	—	1.4	21	—	—	—	Nil
	—	—	1.1	29	—	—	—	
	—	—	1.5	7.7	—	—	—	
	—	—	1.2	8.6	—	—	—	
14-1	—	—	1.5	21	—	—	—	
	—	—	1.0	27	—	—	—	
14-3	—	—	0.9	19	—	Trace	—	Nil
Material used for growing crystals[c]								
247-5-1	5	2	<2	10	4	7	—	K[b]
	<3	1	<2	5	<3	<3	—	K[b]
	—	—	2.2	12	<5	—	—	—
	—	1.3	2.8	13	<5	—	—	—

[a]Limits of detection: Li, 30 ppm; K, 600 ppm; B, 60 ppm; Mn, 2 ppm; Ni, Cr, V, Pb, 5 ppm.

[b]Estimated at 3 to 4 ppm by other laboratory.

[c]Analyses of one typical sample.

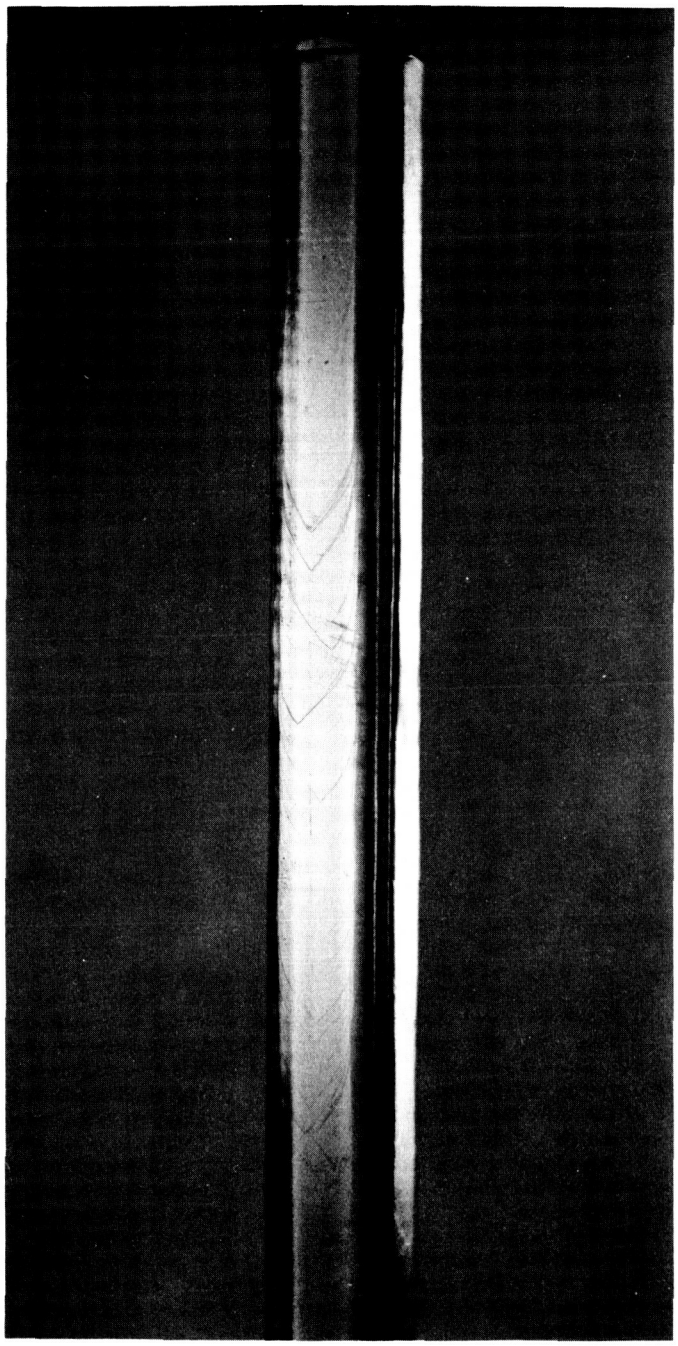

Fig. 3. <100> NaCl crystal rod, showing {100} faces

became somewhat dull as a result of atmospheric etching. Most of the crystals were tested without prior surface treatment (a few were water polished immediately before testing) in the same manner as the cleavages described in B.

As a rule, each crystal rod was cleaved into two or more specimen lengths. In every case, a nearly perfect {100} cleavage was obtained, with little or no deformation (i.e., birefringence) beyond 3 to 4 mm of the cleavage surface. In testing these specimens, care was taken to ensure that the deformed end was well beyond the test area. Special mention must be made of two crystals that were slightly deformed as a result of careless handling during storage (indicated by a slight birefringence pattern throughout the crystal). Specimens from these crystals were water polished prior to testing and are reported separately.

B. Cleavages

A 38- × 50- × 64-mm cleavage of *cleavage quality* optical sodium chloride[1] was cleaved into rods approximately 5- to 6-mm square in cross section. Cleavage was effected by lightly sawing a carefully oriented groove and then cleaving with a light tap on a microtome blade set at a slight angle to the groove; previous experience indicated that this method causes the least plastic deformation.

The as-received crystal block showed a birefringence pattern indicative of 2 orthogonal {100} $<1\bar{1}0>$ slip systems (i.e., a network of intersecting lines, oriented 45 deg to the surfaces of the block, was observed through one pair of cleavage faces while a diffuse birefringence was observed through the others). This pattern was accentuated to varying degrees by further cleaving, in the same manner as reported by other laboratories (Ref. 6). To keep track of the orientation of the initially operative slip systems, the specimens were indexed with reference to their birefringence pattern. Unfortunately, the index marks were in some cases obliterated during subsequent water polishing and orientation of the slip systems had to be made by identification of the specimens from prior photographs; therefore, these predeformation orientations are not entirely reliable.

All cleavages were polished for 20 to 80 min in a 50% hydrochloric acid solution, rinsed in pyridine and dried. They were then annealed for 8 hr in an argon atmosphere at a temperature of 700°C and cooled at a rate of 200°C/hr (this procedure is similar to that used in other laboratories, Refs. 2, 3, and 6). After annealing, all traces of birefringence had disappeared. The specimens were repolished, using the same procedure as before, dried, and stored in a dessicator until testing.

[1]Purchased from the Harshaw Chemical Company, Cleveland, Ohio.

C. Comparison of Crystal Rods and Cleavages

Spectrochemical analyses of all the specimens tested are listed in Table 1. The values reported for aluminum and silicon are somewhat questionable; these elements are unlikely impurities in the NaCl lattice but are invariably present in the carbon electrodes. Moreover, the emission lines of Al and Si are intensified by the presence of volatile halides. The values for the remaining elements reported in Table 1 are probably reliable only as relative concentrations for comparison between specimens. The cleavages appear to have lower concentrations of metal ion impurities than do the crystal rods, but both are of the same order-of-magnitude in overall purity.

No attempt was made to analyze for anionic impurities. Inasmuch as the Harshaw Chemical Company makes an effort to remove all impurities that impair the optical transmission, it may be presumed that the cleavage specimens have lower concentrations of $SO_4^=$, NO_3^-, $CO_3^=$, Br^-, and I^- than do the crystal rods. On the other hand, since the Harshaw crystals are grown in air (to encourage precipitation of metallic impurities), the crystal rods may have lower concentrations of $O^=$. Presumably the predominant anionic impurity is hydroxide ion, which forms at high temperatures from the adsorbed and included water present in all solution-crystallized sodium chloride by the reaction: $NaCl + H_2O \rightarrow NaOH + HCl$ (Ref. 16). Otterson (Ref. 17) has found that appreciable concentrations of OH^- are present in all sodium chloride crystals grown from melt. Since no attempts to remove this ion (e.g., by treatment with dry HCl) were made, either upon the Harshaw material or the crystal rods, it is presumed that comparable concentrations of OH^- are present in all specimens.

Dislocation densities were measured by etch-pit counts. These measurements were not made on the test specimens, which might have been scratched or bent during microscopic examination, but on comparable crystal rods and cleavages prepared in an identical manner. Specimens were etched by Mendelson's technique (Ref. 18) and rinsed in pyridine. Photomicrographs were taken and the etch-pits counted by a semiautomatic method (Ref. 19). The dislocation densities ranged from 1.3×10^6 to $5.0 \times 10^6/cm^2$ for a typical cleavage and averaged $1.25 \times 10^6/cm^2$ for the crystal rods. Therefore, it may be assumed that the dislocation densities are of the same order-of-magnitude for both types of specimens.

A photomicrograph of the etch-pit pattern of a typical crystal rod is shown in Fig. 4. A well-defined substructure of low-angle boundaries is visible as single-line arrays of dislocations; few dislocations are observed within individual crystallites. In contrast, the etch-pit pattern of annealed cleavages (Fig. 5) appears to be more diffuse and random. However, X-ray diffraction topographs of typical Harshaw cleavages indicate a substructure of 1- to 2-mm crystallites with a mutual misorientation of 1 to 2 min of arc (Ref. 20); this is qualitatively comparable to the etch-pit structure of the crystal rods.

The cross sections of all specimens tested are shown in Fig. 6. It will be noted that the crystal rods tend to be more rounded and of smaller cross section than most of the annealed cleavages, but, as will be shown, the differences do not appear to be sufficient to affect a comparison of the mechanical properties.

The surfaces of both types of specimens are, as a rule, microscopically smooth. Occasionally, however, the crystal rods have growth steps such as are shown in Fig. 4. It has been suggested that such steps can act as stress-concentrating notches and thereby reduce the overall ductility (Ref. 11).

In summary, except for predeformation, most of the differences between the crystal rods and the annealed cleavages appear to be of little consequence except possibly for dislocation density and metallic ion impurity concentrations. Moreover, there appears to be less variation among the cleavages than among the crystal rods, so that a greater range of idiosyncrasies in the mechanical behavior of the cleavages would seem to be validly attributable to the effects of predeformation.

D. Testing Procedure

The specimens were tested in flexure, not only to eliminate the problem of deformation-free gripping, but also because one of the most striking types of idiosyncrasy—soft vs stiff behavior—has been reported only for bend tests (Refs. 5 and 6).

The test fixture is shown in Fig. 7. Four-point loading was used so as to produce uniform stress in the region of maximum deformation. The lower load members were spaced 30 mm apart and the upper load members 10 mm apart. All load members were 3.175 mm (⅛ in.) hardened steel rods which, in accordance with the admonition of Rothwell and Greenler (Ref. 6), were so fitted into their mountings as to be capable of free rotation, thereby minimizing tensile or compressive stress contributions (ball bearing mounts could not be used because of their

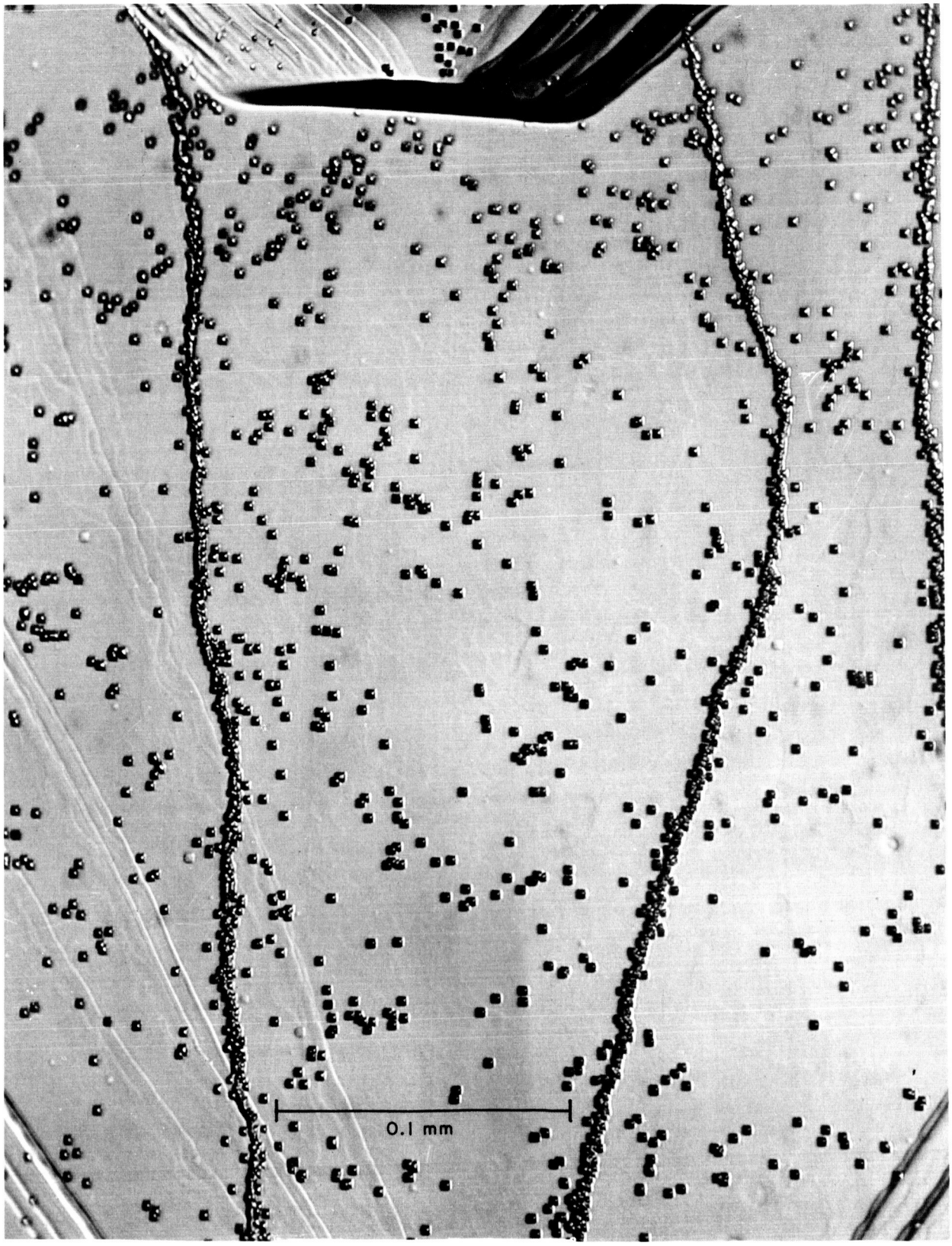

Fig. 4. Typical etch-pit patterns of NaCl crystal rods

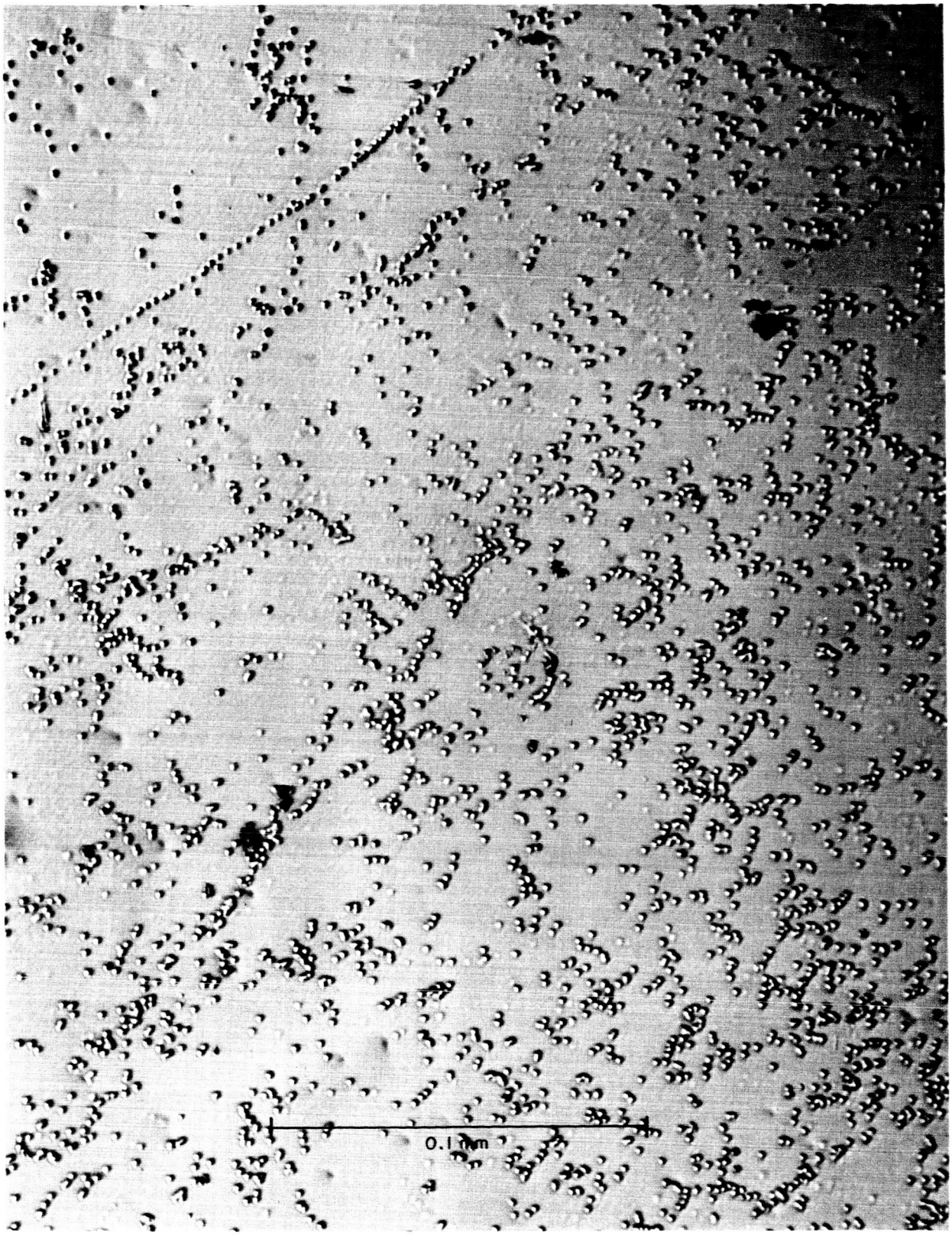

Fig. 5. Typical etch-pit patterns of annealed cleavages of NaCl

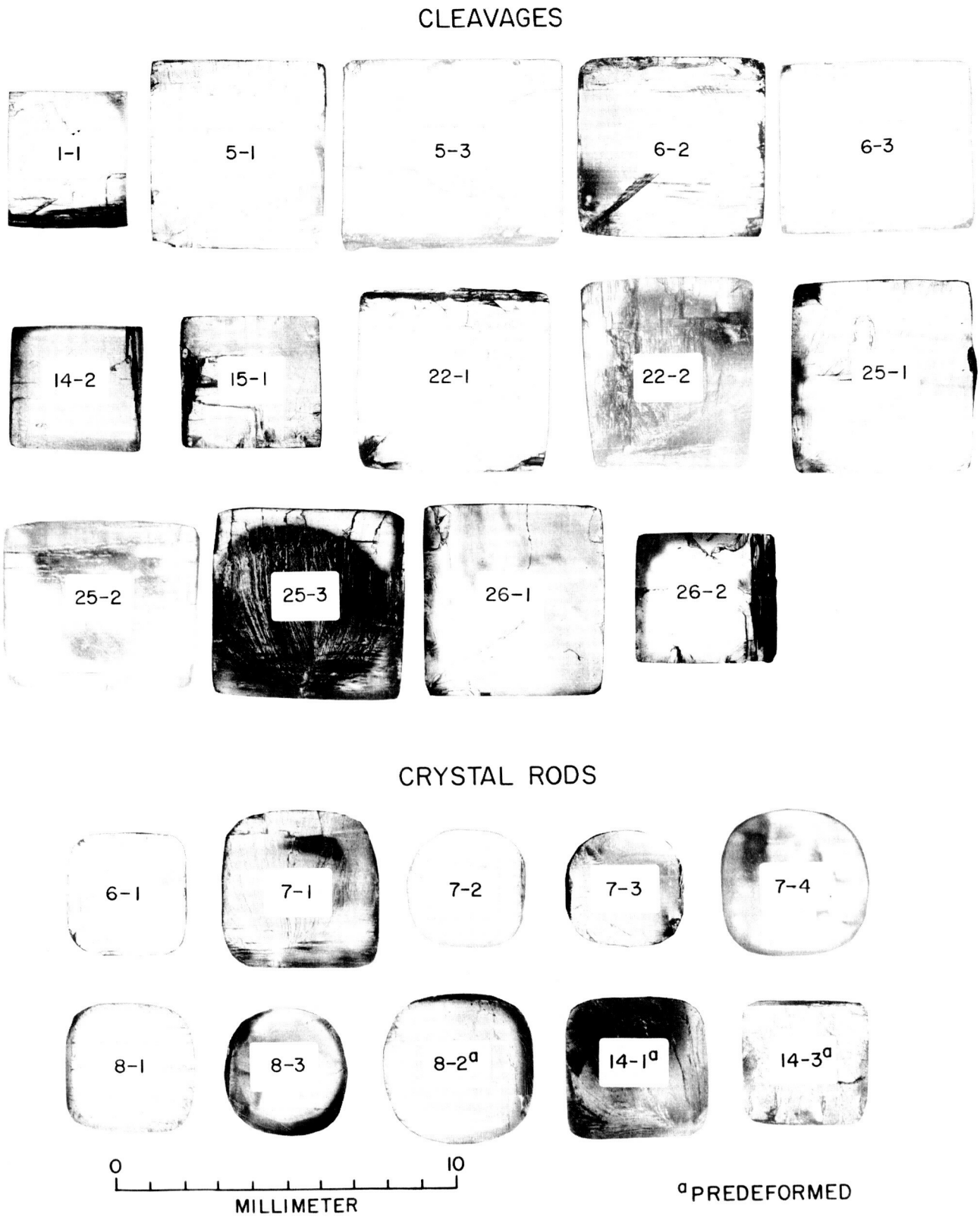

Fig. 6. Cleavage cross sections of bend-test specimens of NaCl crystal rods and annealed cleavages

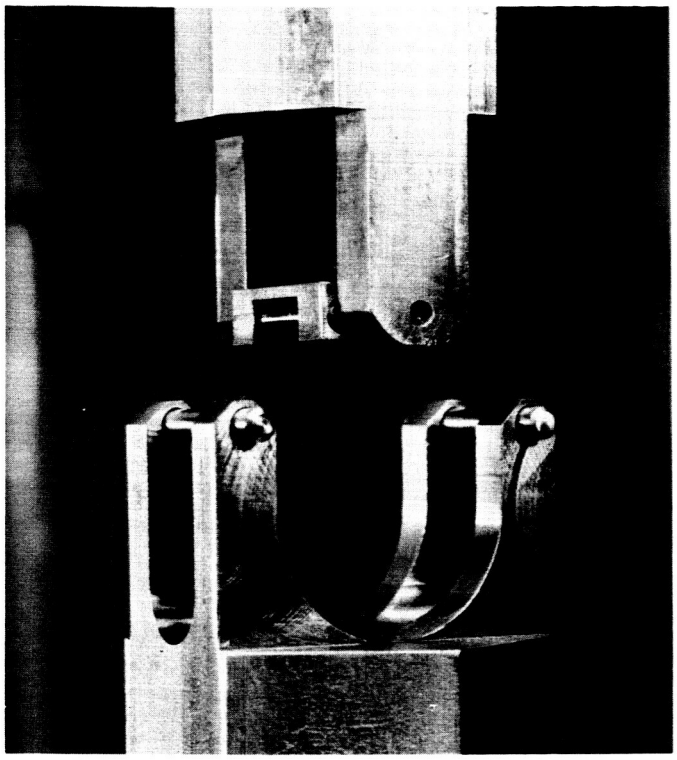

Fig. 7. Jig used for bend tests

interference with polarized-light photography of the specimens during deformation). As a further precaution, the upper load members were mounted on a central pivot to ensure equalization of loading.

Before each test, the upper and lower parts of the test fixture were aligned and centered with respect to each other. The specimen was then inserted, with a flat {100} surface resting on the lower members, and aligned in a similar manner. The cleavage specimens were also oriented with reference to the predeformation slip systems that had been observed as birefringence lines before annealing. Specimens in one group (A) were oriented so that the pairs of orthogonal slip systems activated by predeformation were also those activated during the bend test; these specimens were expected to exhibit soft behavior. The other group of specimens (B) were oriented so that the predeformation slip planes were vertical and, therefore, nonorthogonal to the slip systems activated by testing; this group was expected, on the basis of latent hardening effects and the observations of Rothwell and Greenler (Ref. 6), to exhibit stiff behavior.

Bend tests were conducted on a table model Instron (Model TM-M-L) testing machine. The strip chart recorded load vs time which, for the tests described, could be reliably equated to load vs true deflection. Experiments with metal strips and 2-in. steel bars, in the specimen position, confirmed the assumption that load-cell deflection, cross-head deflection, and irregularities in deflection rate and chart speed could be ignored. All tests were conducted at deflection rates of 0.05 mm/min; this is equivalent to outer-fiber strain rates of 1.5 to 3×10^{-5}/sec. This slow rate was chosen to permit accurate recording of abrupt changes in load; bending specimens by hand indicated that, at least in the case of the crystal rods, far higher deformation rates could be employed without substantial change in mechanical behavior. For this reason also, differences in true outer-fiber strain rate, caused by testing specimens of varying thicknesses, could be ignored. Tests were stopped either at the first sign of fracture or when the specimen had been bent in a 90-deg arc (15 to 20% outer-fiber strain), since, at these high deflections, the tests ceased to have quantitative significance.

The parameters of testing were measured in the usual manner. The load (L) was measured directly from the strip chart. The deflection (D) was equated to chart length × machine deflection rate ÷ chart drive rate and was accordingly measured directly from the chart. The cross-section moments of inertia (I) and the outer-fiber distances (h) were measured graphically. After testing, each specimen was cleaved in or near the region of maximum deflection. Photomicrographs of these cross sections (Fig. 6) were then superimposed on a translucent x vs y^3 grid (Fig. 8). Since the moment of inertia for any one vertical column from the centroid is equal to $xy^3/3$, the total number of grid boxes contained within the specimen cross section equals thirty times the moment of inertia. The cross-section photomicrograph was in each case positioned so as to contain an equal number of boxes above and below the centroid; this is equivalent to the assumption of pure bending. This method of estimating I was found to be accurate within $\pm 5\%$. In a similar manner, the outer-fiber distance (h) was measured as the average of the maximum distances from the centroid to the upper and lower edges.

E. Other Measurements and Tests

After completion of the bend tests, the radius of curvature (R) and the thickness ($\simeq 2\,h$) of each specimen were, whenever feasible, measured directly with an optical comparator. The measurement of R was so lacking in precision (about $\pm 10\%$) that the resultant calculations of outer-fiber strain at termination of test ($E_f' = h/R$) can only be regarded as approximate confirmations of the

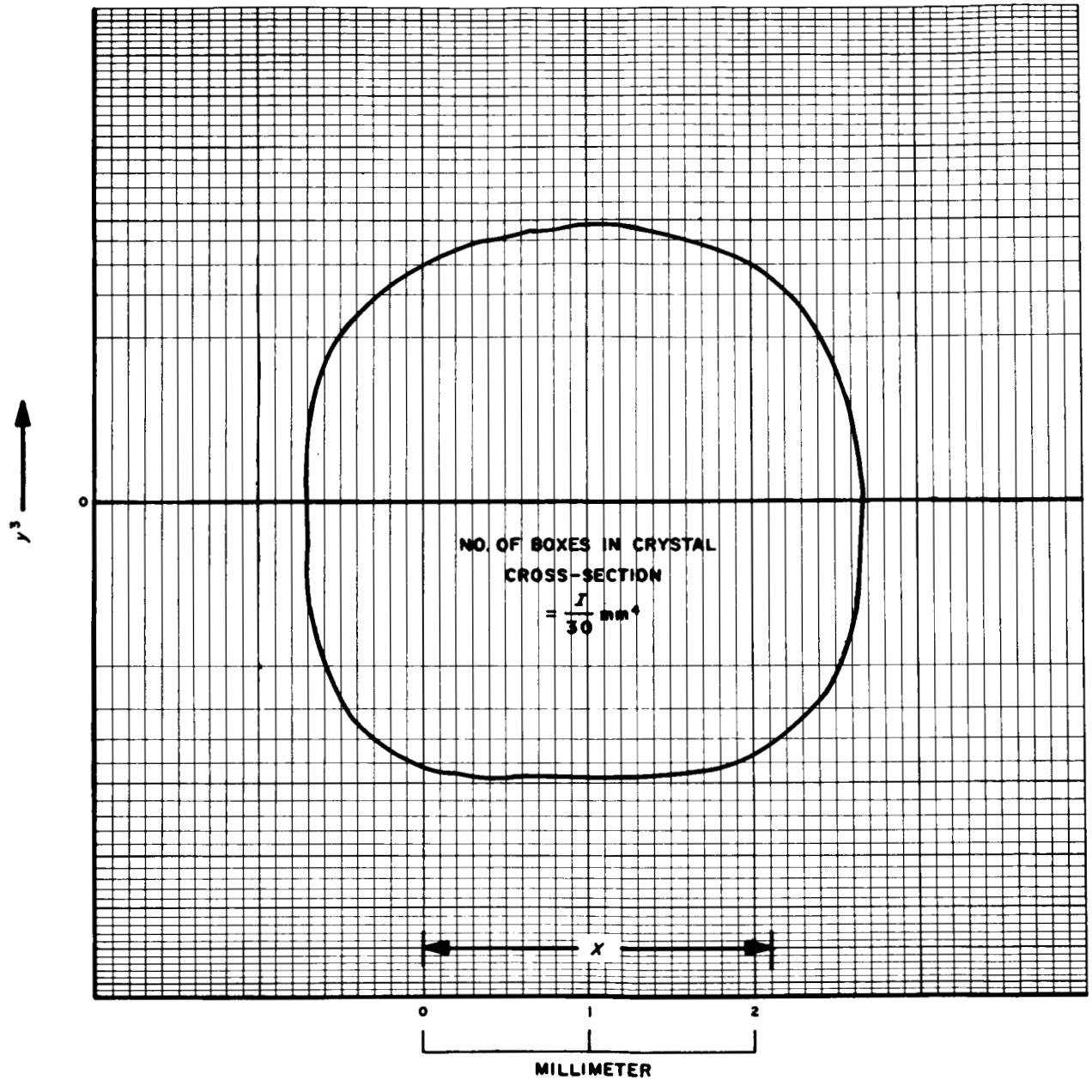

Fig. 8. Grid (x vs y^3) showing estimates of moment of inertia

elastic-equivalent outer-fiber strain at termination of test E_f. Specimens were also examined for slip bands, localized deformation near load members, and any other significant visible features.

Preliminary to the preceding tests, crystals and cleavages were bent by hand under varying conditions of rate and environment and after various pretreatments. The results of these tests are reported in the next Section.

III. DATA REDUCTION[a]

In comparing bend tests of specimens with different cross sections, some authors prefer to plot the unreduced instrumental data (Refs. 2 and 10). This was considered disadvantageous for the data presented in this Report, inasmuch as variations in the load-deflection curves, caused by variations in the I or h of the different specimens, might be so great as to obscure any real idiosyncrasies. On the other hand, a detailed plastic-deformation analysis of each test would have been not only difficult and time-consuming, but also unwarranted by the precision of the tests and measurements. Therefore, as a compromise, the assumption of quasi-elastic behavior was made. An elastic-equivalent outer-fiber shear stress (T) and an elastic-equivalent outer-fiber strain (E) were calculated. Under conditions of purely elastic deformation, T and E would be equivalent to the true outer-fiber shear stress (resolved along $<1\bar{1}0>$ on the {110} slip planes) and the true outer-fiber tensile strain in the region of uniform maximum deformation (i.e., between the inner load members).

In pure elastic bending, $S = Mh/I$, where S is the tensile stress on the outer-fiber of the beam, M is the bending moment, h is the distance from the neutral axis to the outer fiber, and I is the moment of inertia of the cross-section area about the neutral axis (Ref. 21). In four-point loading, the bending moment is equal to the product of the load on one inner member, $L/2$, and the distance between the inner and outer member, a (i.e., $m = La/2$, Ref. 22). The outer-fiber tensile stress is related to the resolved shear stress, T, as $T = S \cos \Phi \cos \lambda$ (Ref. 23). In the present case, Φ (the angle between the slip-plane normal and the axis of tension) and λ (the angle between the slip direction and the axis of tension) are both 45 deg.

Combining these equations we obtain:

$$T = \frac{Lah}{4I} \tag{1}$$

The machine deflection, D, is assumed to be equivalent to the specimen deflection at the inner load member. For the testing fixture used here, and again assuming pure elastic bending, this equals (Ref. 22):

$$D = \frac{5La^3}{12YI} \tag{2}$$

where Y is the elastic modulus. Since $Y = S/E$ (assuming Hooke's law) and, from the previous equations, $S = Lah/2I$ then:

$$E = \frac{6Dh}{5a^2} \tag{3}$$

Since, for each specimen, $T \propto L$ and $E \propto D$, the elastic-equivalent stress-strain curves could be obtained by merely rescaling the ordinates and abscissas of the strip chart load-deflection curves. The resultant curves are shown in Figs. 9 through 14.

The pertinent parameters of the bend tests are summarized in Table 2. These include in addition to those already described:

- $w/2h$ the width-to-thickness ratio of the cross section of the specimen
- T_y the elastic-equivalent outer-fiber <110> resolved shear stress at the yield point, which is presumed to be the first detectable deviation from linear elastic behavior, excluding initial anelastic feet
- G_I the average slope of the stress-strain curve, dT/dE, during the *first stage* of plastic deformation; e.g., between the yield point and the onset of increasing slope. (This quantity is obviously somewhat subjective but is probably reliable within ±5%. It provides some indication of the rate of work hardening as deformation increases, but should not be confused with the standard work-hardening rate that would be obtained from the true-stress/true-strain of a tensile test.)
- E_f the elastic-equivalent strain at fracture or at termination of the test as calculated from Eq. (3)
- E_f' the outer-fiber strain at fracture or at termination of the test as measured directly from the thickness ($2h$) and radius of curvature, R, of the specimen, i.e.,

$$E_f' = h/R \tag{4}$$

Before discussing the results of these tests, it is first necessary to use the data to examine the validity of the assumptions used in data reduction. A plot of E_f vs E_f'

[a]For a definition of terms, refer to page 29.

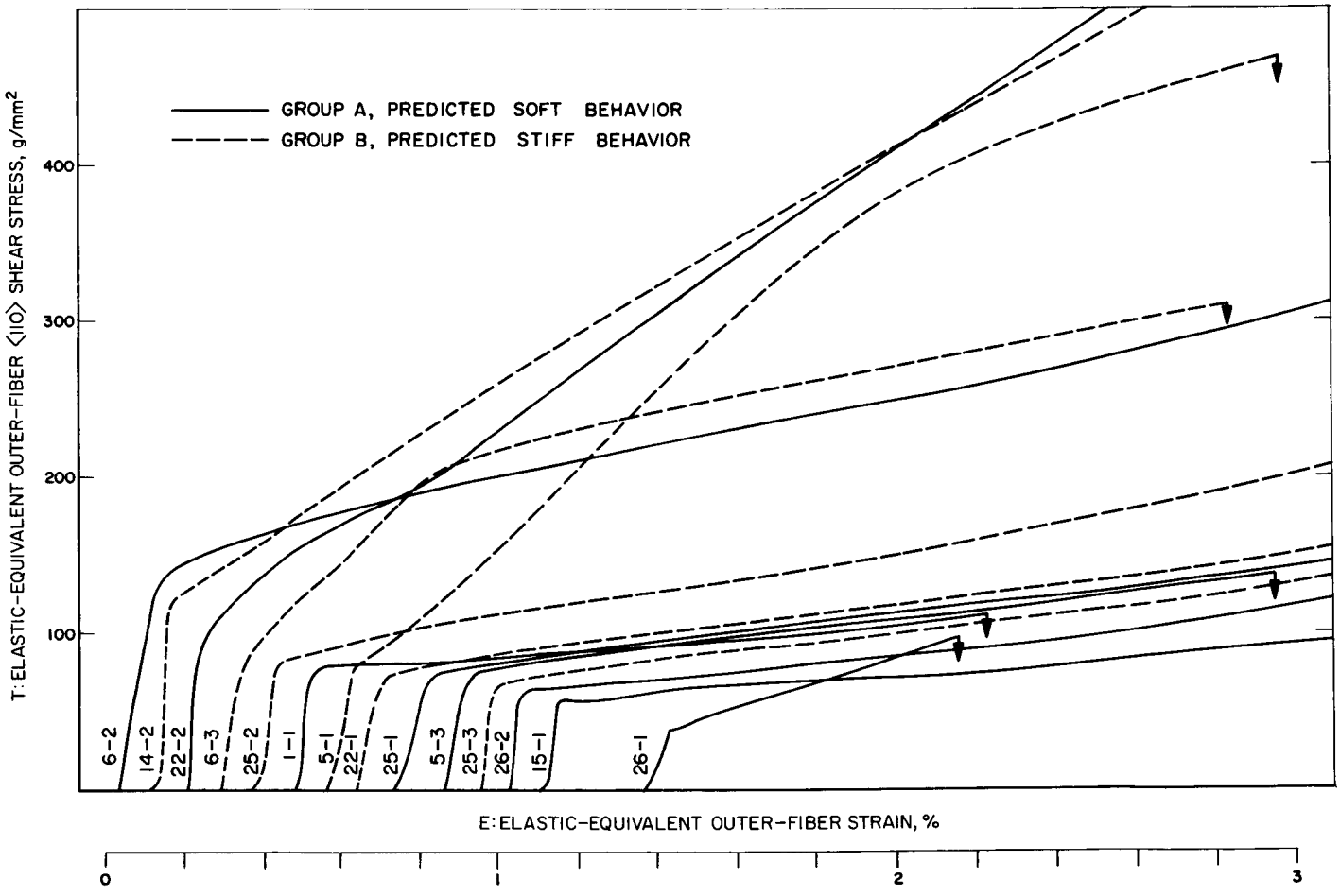

Fig. 9. Elastic-equivalent stress-strain curves for annealed cleavages of NaCl (0 to 3% strain)

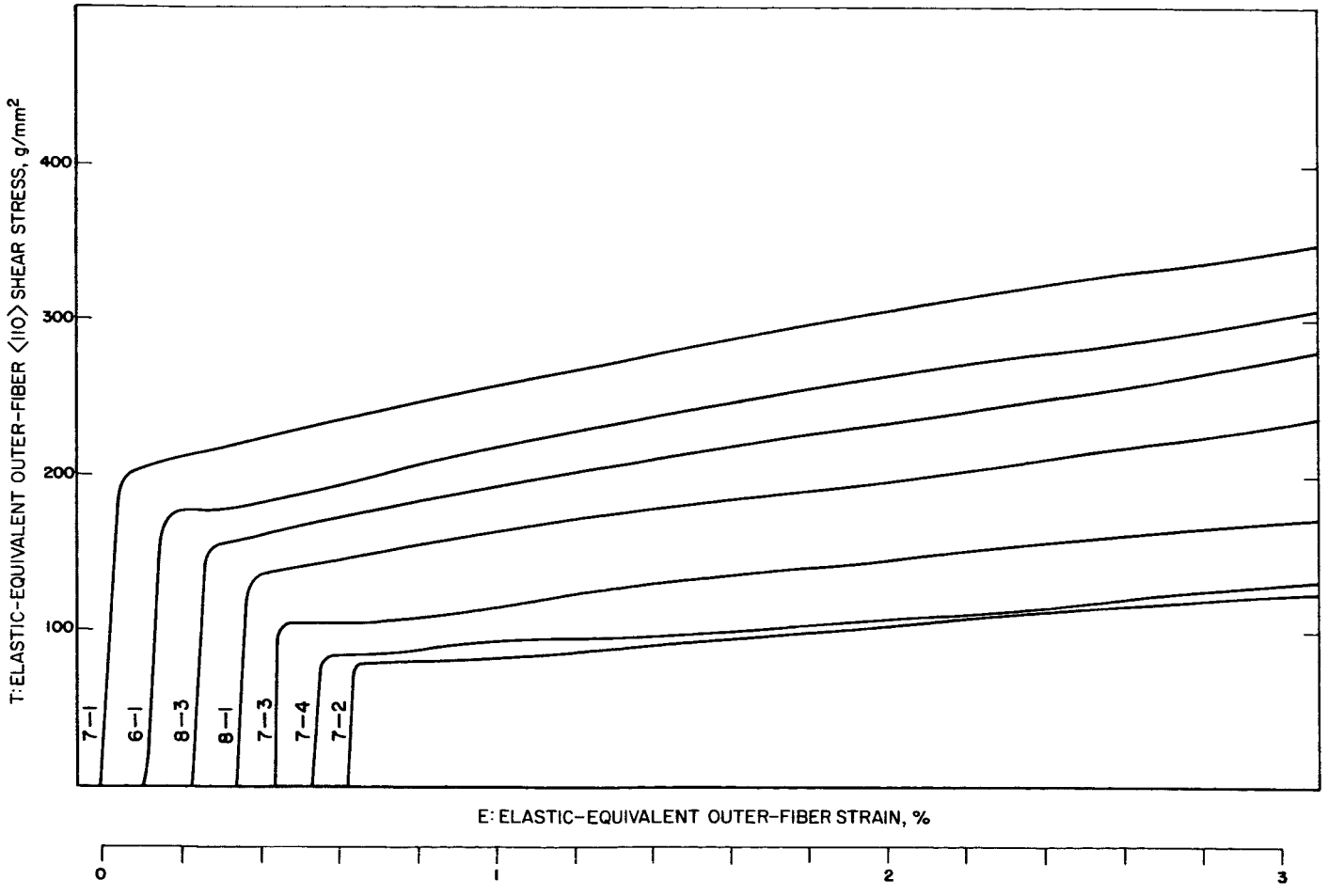

Fig. 10. Elastic-equivalent stress-strain curves for as-grown NaCl crystal rods (0 to 3% strain)

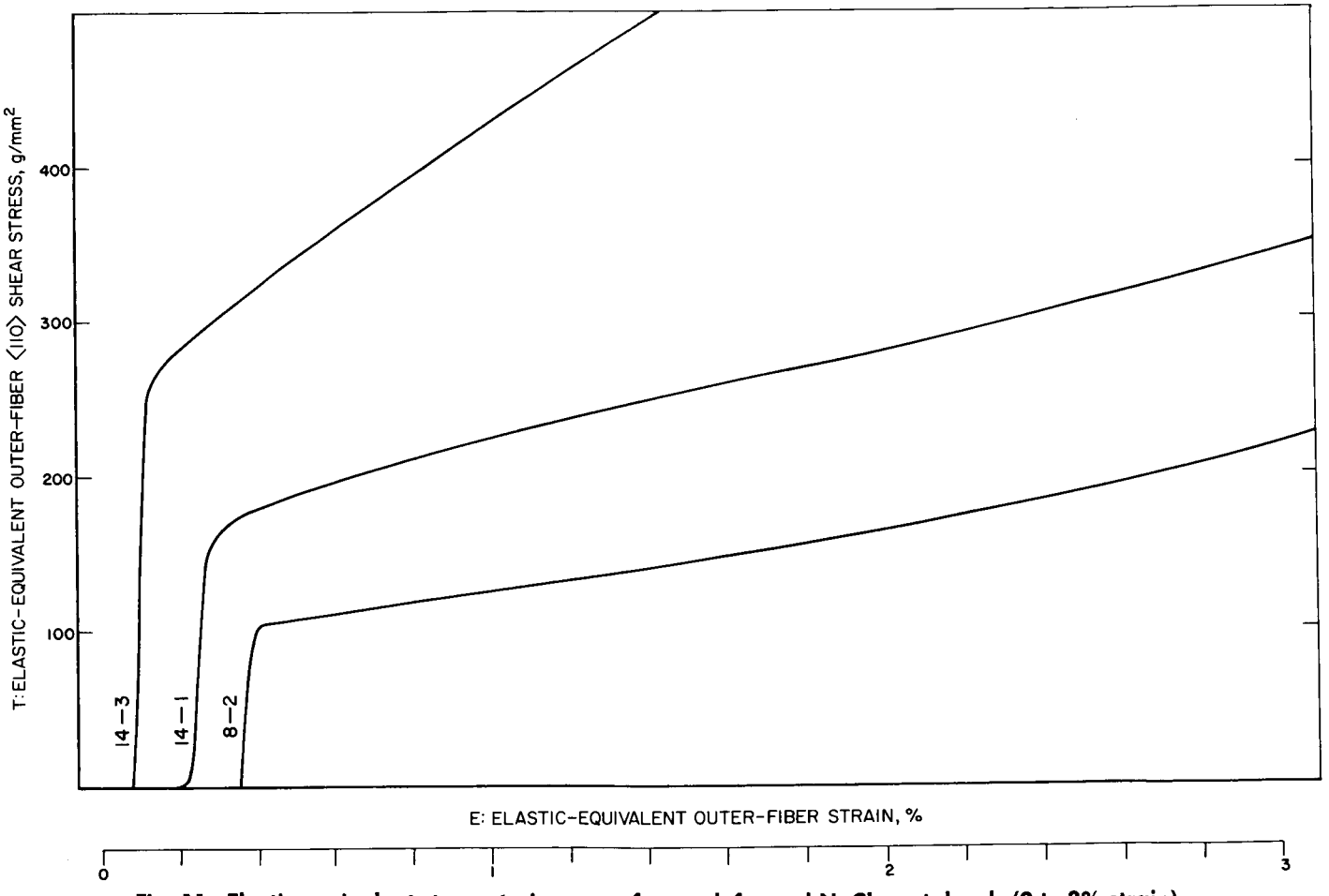

Fig. 11. Elastic-equivalent stress-strain curves for predeformed NaCl crystal rods (0 to 3% strain)

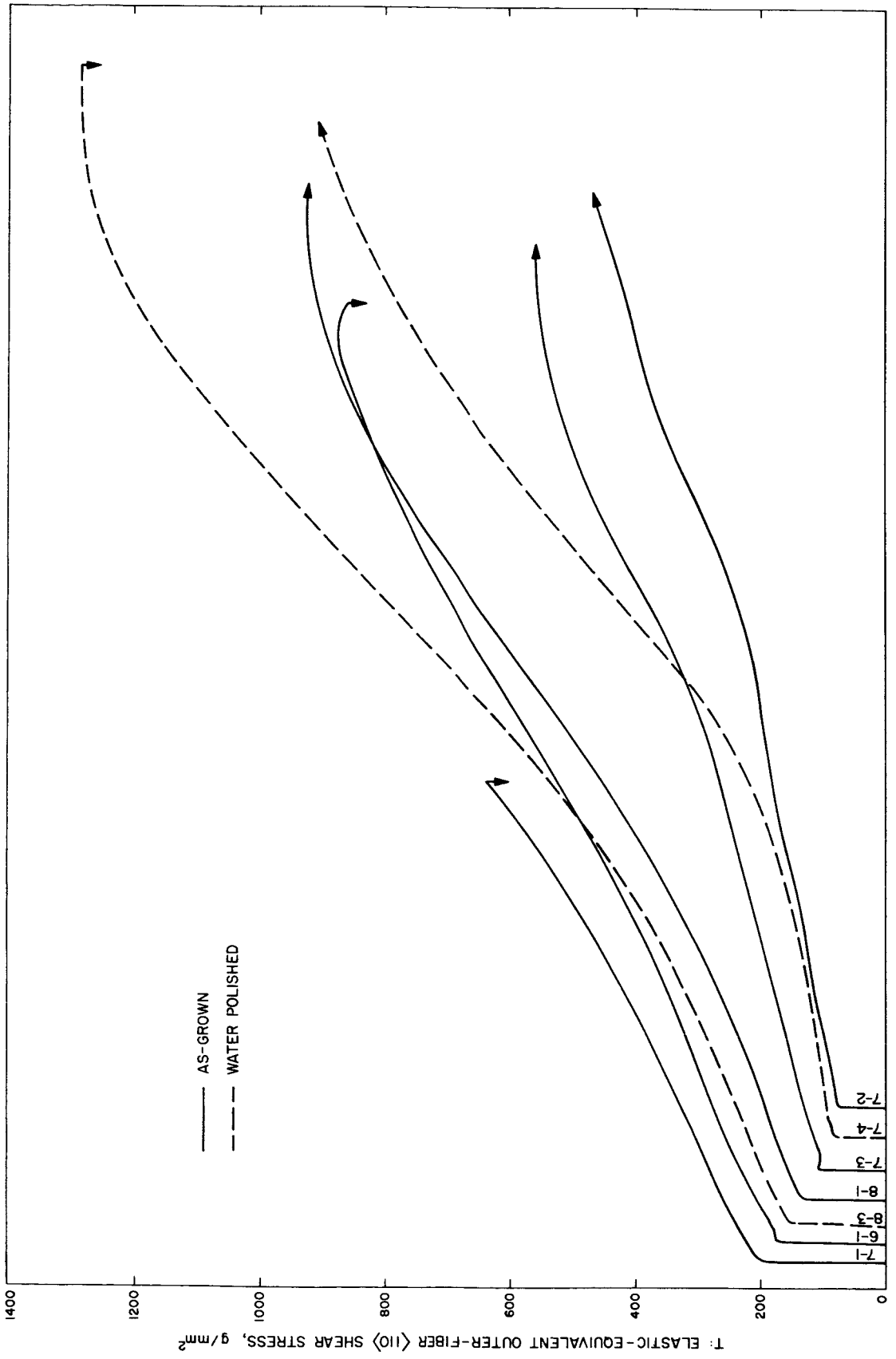

Fig. 12. Elastic-equivalent stress-strain curves for as-grown NaCl crystal rods (complete tests)

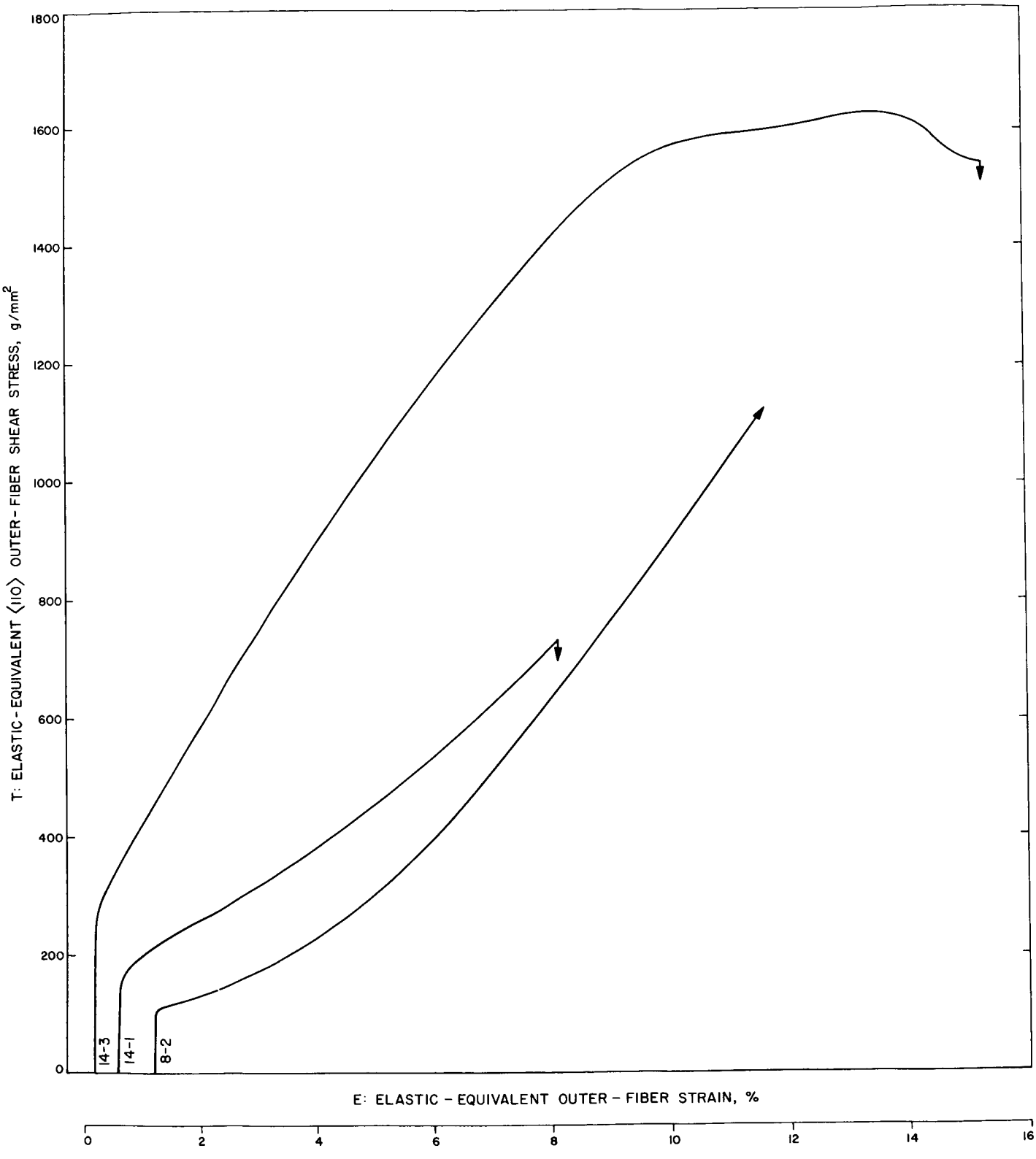

Fig. 13. Elastic-equivalent stress-strain curves for predeformed NaCl crystal rods (complete tests)

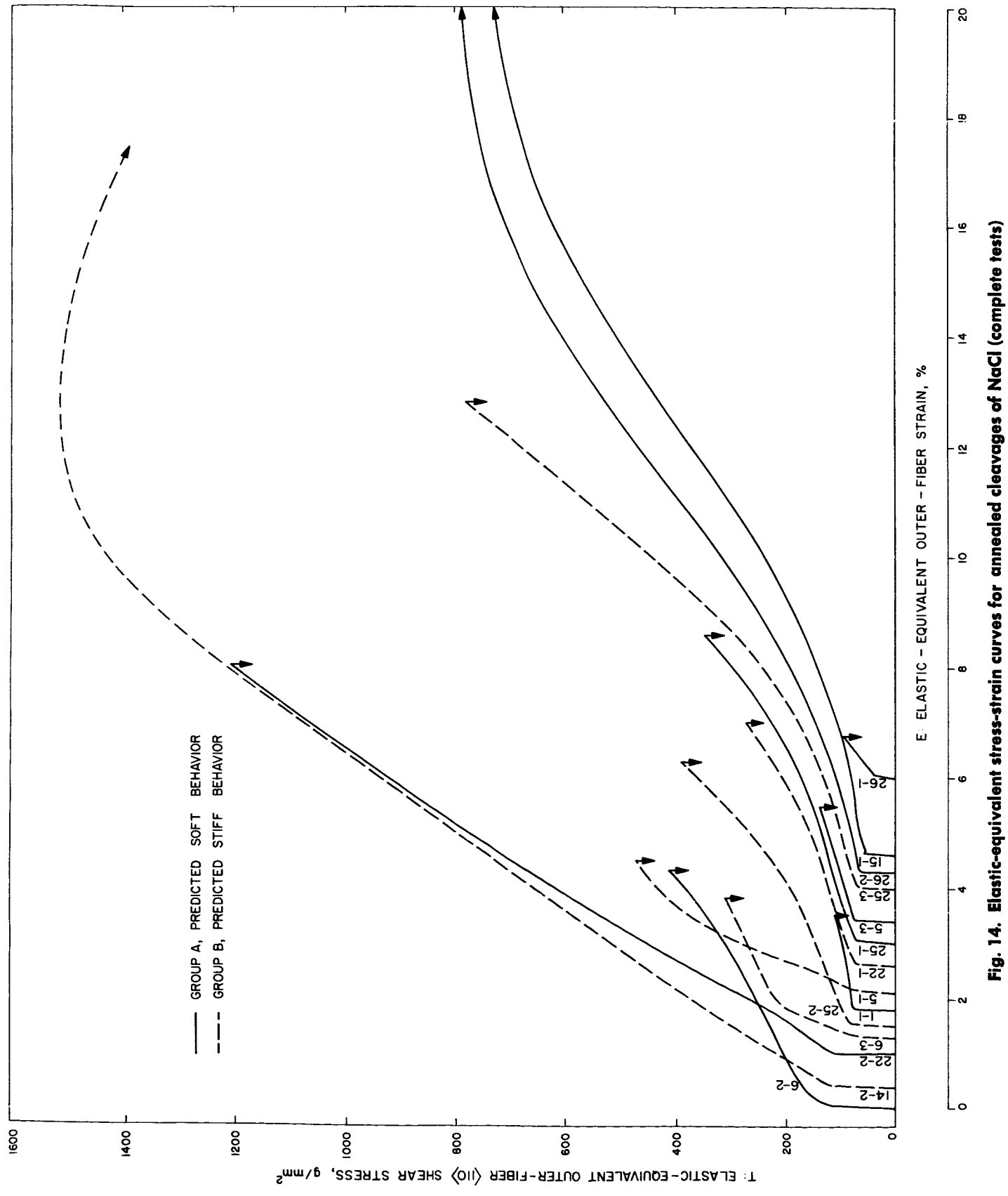

Fig. 14. Elastic-equivalent stress-strain curves for annealed cleavages of NaCl (complete tests)

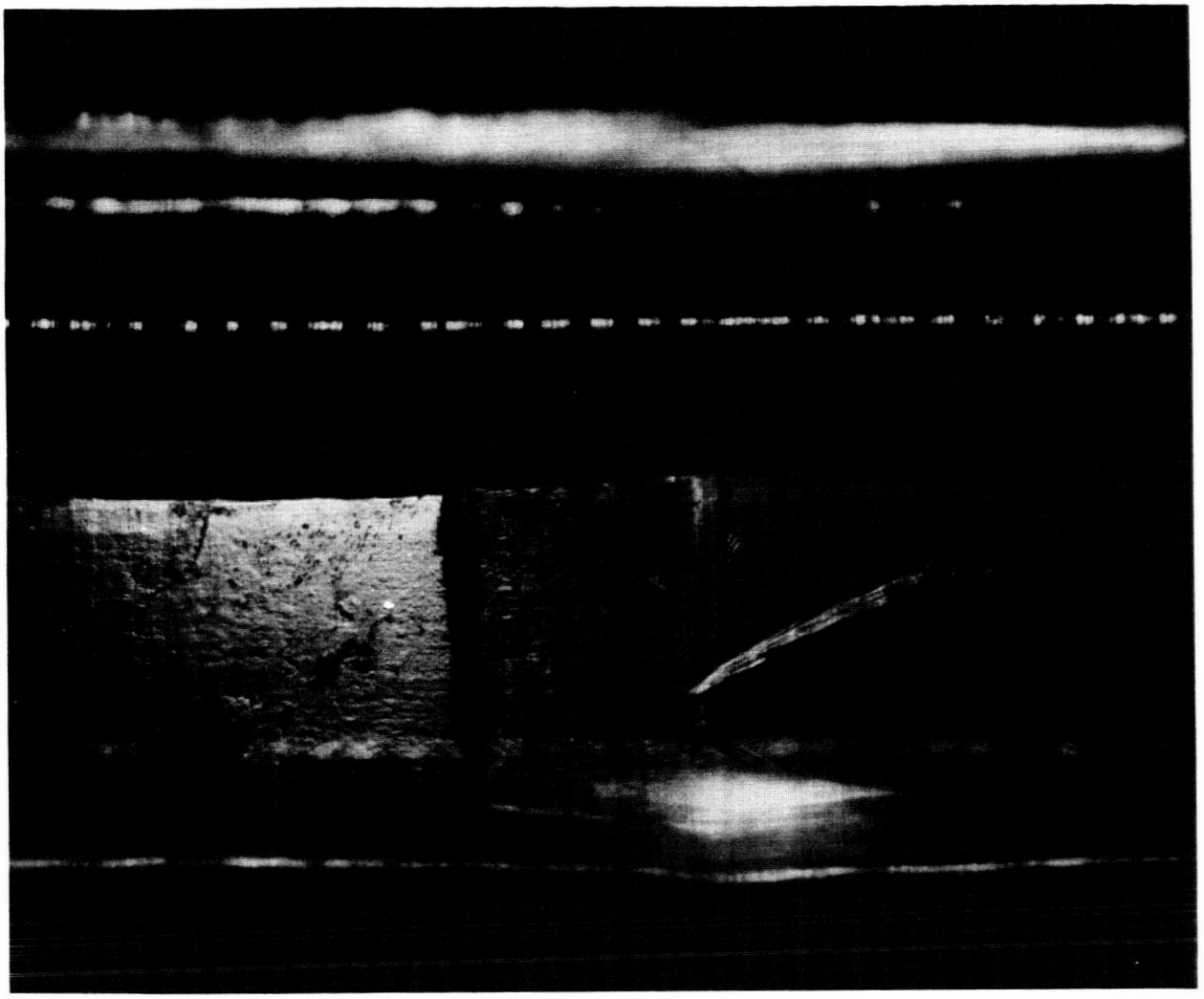

Fig. 15. Localized abrasion and deformation on NaCl bend-test specimen due to movement of crystal against load member

shows good agreement for strains below 10% but indicates a systematic discrepancy at higher strains, the E_f becoming anomalously high. The primary requirement (i.e., that T and E be independent of the size or shape of the specimen) was tested by plotting T_y and G_1 against the geometric parameters of the specimens: I, h, and $w/2h$. In no case was there any sign of a correlation or trend. It therefore seems safe to assume that, for the first few percent of strain, T and E are reliable approximations of the true stress and the true strain.

At higher strains, however, when the specimen is curved into a visible arc, there are inevitable geometric complications. The deflection, D, and the load member spacing, a, must be corrected for the finite thicknesses of the specimen and the load members. Moreover, even with rotating load members, there is a tendency for localized stress concentration and deformation where the specimen touches the load members. The existence of these effects in the tests presented in this Report is shown in Fig. 15, which shows abrasion and deformation where the specimen rubbed against the outer load member, and Fig. 16, which shows irregularities in the birefringence pattern of bent specimens. An additional complication arises from the cross-sectional shape of the specimen. Round specimens tend to fracture more easily than square specimens, due to the development of anticlastic kink boundaries near the corners (Ref. 24). For all of these reasons, the values of T and E at high strains must be regarded as having qualitative significance only and comparisons should only be made between specimens of nearly identical size and shape.

Table 2. Results of bend tests of NaCl cleavages and crystal rods

Specimen	Pretreatment[a]	l, mm^4	h, mm	$w/2h$	T_y, $\frac{g}{mm^2}$	G_f, $\frac{g}{mm^2}$	E_f	E'_f	K
Cleavages									
1-1	A a	17.4	1.98	0.86	73	1.6×10^3	0.018		29
5-1	B a p	65.3	2.72	0.93	75	24.2	0.024		424
5-3	A a p	85.1	2.79	1.15	70	2.8	0.021		54
6-2	A a p	61.8	2.63	1.04	128	5.8	0.035		53
6-3	B a p	52.4	2.50	1.13	77	24.2	0.025		410
14-2	B a p	14.9	1.87	1.05	115	15.6	>0.174[b]	>0.140[b]	161
15-1	A a p	18.3	1.92	1.06	55	1.9	>0.168[b]	>0.144[b]	51
22-1	B a p	69.9	2.69	1.03	70	3.5	0.044		87
22-2	A a p	62.8	2.83	0.90	75	16.8	0.070		295
25-1	A a p	70.3	2.81	0.94	68	3.1	0.056		62
25-2	B a p	48.2	2.45	1.14	75	4.1	0.048		71
25-3	B a p	71.5	2.77	1.00	60	3.2	0.088		76
26-1	A a p	72.9	2.80	0.94	40	8.5	0.076		296
26-2	A a p	17.2	1.92	1.07	57	2.5	>0.173[b]	>0.152[b]	64
As-grown crystal rods									
6-1		10.4	1.76	0.96	162	4.5	0.150	0.131	31
7-1		28.3	2.39	0.99	193	5.0	0.076	0.081	29
7-2		7.9	1.70	1.00	75	2.0	>0.141[b]	>0.100[b]	35
7-3		7.5	1.72	1.02	100	2.7	>0.148[b]	>0.115[b]	33
7-4	p	19.4	2.15	1.00	80	1.9	>0.161[b]	>0.123[b]	31
8-1		13.0	1.87	1.00	123	3.8	>0.159[b]	>0.140[b]	36
8-3	p	19.4	2.12	0.96	147	4.5	0.200	0.173	35
Predeformed crystal rods									
8-2	p	20.8	2.22	0.99	105	3.3	0.105[b]	0.097[b]	37
14-1	p	19.8	2.06	0.99	150	6.1	0.076	0.071	46
14-3	p	13.0	1.81	1.00	255	17.0	0.183	0.146	72

[a] A = predicted *soft* behavior
B = predicted *stiff* behavior
a = annealed
p = water polished

[b] Specimen that did not fracture

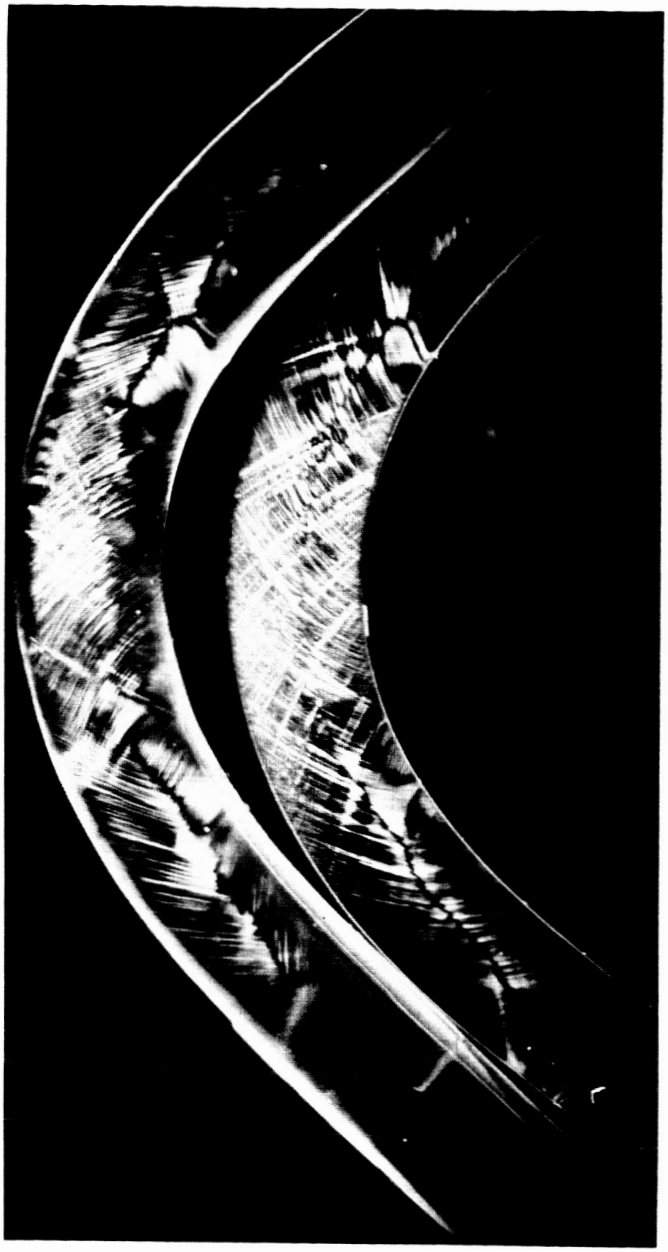

Fig. 16. Birefringence patterns of NaCl bend-test specimens

IV. RESULTS

The early stages of deformation of the annealed cleavages (Fig. 9) exhibit all of the idiosyncrasies reported by other authors. Several of the curves have prominent anelastic regions in the initial stage of deformation; others have kinks or irregularities in shape near the yield point. The yield stress varies between 60 and 80 g/mm^2 for most specimens; however, in a few cases, the yield stress is much higher or lower.

The most prominent idiosyncrasy is the variation in G_I. The specimens tend to be divided into two distinct groups: (1) those exhibiting soft behavior ($G_I < 6 \times 10^3$), and (2) those exhibiting stiff behavior ($G_I > 8 \times 10^3$). A comparison of G_I with the predicted behavior on the basis of predeformation birefringence (groups A and B) shows a significant correlation. The average G_I is 5.4 for group A, and 12.5 for group B. A possibly more meaningful empirical correlation factor is $K = G_I (T_y - 18)$, which is approximately constant for the as-grown crystals. The average value of this factor is 113 for group A, and 205 for group B.

In contrast to the erratic curves of the cleavages, the as-grown crystal rods (Fig. 10) behave in a much simpler manner. There are no indications of initial anelastic deformation and few, if any, irregularities. Each crystal has a sharp yield point and a linear region of easy glide. There is considerable variation in T_y and G_I, but even these quantities are apparently linearly related (Fig. 17) so that there seems to be only one parameter of variation; according to the equation:

$$G_I = K (T_y - 18) \tag{5}$$

where $K \simeq 33.5$.

Of especial significance is the behavior of the predeformed crystal rods (Fig. 11). These show the anelastic region and wide variation in G_I characteristic of the cleavages. As shown in Fig. 17 and Table 2, K varies by almost a factor of two. Thus, the quantity $(K - 33.5)$ appears to be a crude empirical measure of the amount of work hardening caused by predeformation.

As has been previously mentioned, even qualitative comparisons of the T vs E curves at high deformations (Figs. 12 through 14) should be made with caution. Nonetheless, there are a few prominent features worth noting. The curves for the as-grown crystals (Fig. 12) are all quite similar. All have a linear region of easy glide, a well defined transition (at $E = 5.5$ to 8%) to a steeper linear region and a third region of gradually diminishing slope. These appear to be analogous to the stages I, II and III of deformation of sodium chloride crystals in compression as reported by Davidge and Pratt (Ref. 25). Surprisingly, the water-polished crystals have a steeper

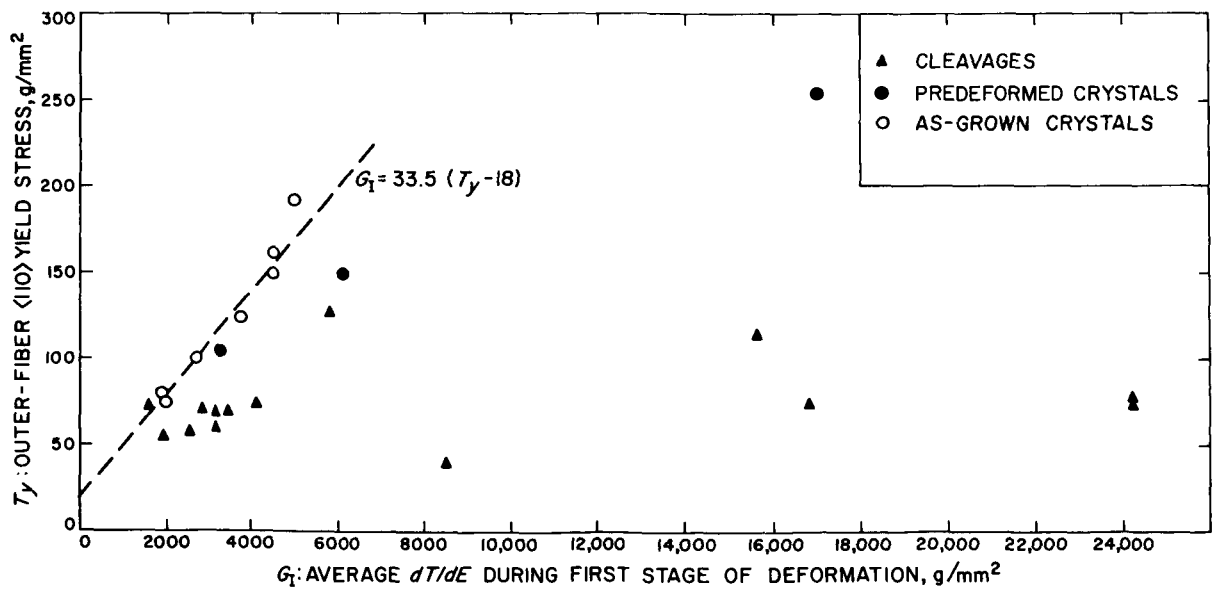

Fig. 17. Variation of T_y and G_I for NaCl bend-test specimens

slope in the second stage of deformation; this suggests that a water-polished surface acts as a greater barrier to dislocations or slip bands than does the as-grown surface.

In contrast to the as-grown crystals, the predeformed specimens (Fig. 13) and, with a few exceptions, the cleavages (Fig. 14) have higher slopes throughout the course of their deformation. Moreover, the predeformed crystals and cleavages fall into two distinct groups: (1) those having either a second stage of deformation with a higher slope than the first stage (e.g., predeformed crystal 14–1 and cleavages such as 22–1) or having a continuous increase in slope, e.g., cleavage 26–2 (a behavior not unlike that of the as-grown crystals); and (2) those having a second stage of deformation with a lower slope than the first, e.g., predeformed crystal 14–3 and cleavages 5–1, 6–3, 14–2, and 22–2. In these latter cases, the onset of the second stage varies widely from one specimen to another, occurring at strains of ½ to 8%. This apparent inversion of the relative slopes of stage I and stage II deformation appears to be the most characteristic difference between soft and stiff behavior.

Another surprising feature is the lack of correlation of early-stage work hardening with ultimate ductility. Some crystals and cleavages with high K values were deformed to strains of 15% or more, whereas some of the "softest" cleavages fractured below 5% strain.

At first glance, the as-grown crystals seem to have far higher ductility than the cleavages. With the exception of specimen 7–1, the average E_f of the as-grown crystals was in excess of 16% with four of the 6 specimens remaining unbroken throughout the test. In contrast, the average E_f of the cleavages (excluding unpolished specimen 1–1) was 7.2% with only three specimens surviving elastic-equivalent strains of 17% or higher. We may, therefore, assume that the cleavages have lower ductility than the as-grown crystals because of cleavage-induced surface damage; however, there is an alternative explanation. An examination of Table 2 shows that the cleavages were, on the average, considerably larger than the crystal rods (the average h values being 2.48 and 1.86 mm, respectively). Significantly, the three most ductile cleavages, each having an E_f more than twice as high as any other cleavage, are also the three smallest cleavages, having an average h of 1.90 mm. Moreover, the only as-grown crystal which fractured below 15% strain (specimen 7–1) was also the largest.[3] This coincidence is too strong to ignore, and additional experiments will be necessary to determine whether ultimate ductility depends primarily on cleavage damage or specimen size.

In addition to the aforementioned data, the following qualitative observations were made:

1. Several of the bent crystal rods exhibited distinct slip bands on the compressively deformed surface (Fig. 18).
2. The crystal rods are greatly embrittled by scratching the surface with sandpaper or by cutting a groove with a razor blade. Even under these circumstances, however, there is some localized plastic deformation before fracture.
3. Macroscopic solid inclusions (e.g., graphite particles from the crucible) caused no obvious impairment of ductility.
4. Crystals that were deformed slightly seemed to be extremely brittle when tested several days later.
5. The ductility of the crystal rods is not obviously rate sensitive. Some specimens were bent to strains of 15% or more within five seconds.
6. Although the as-grown crystals showed no enhancement of ductility by prior water polishing, they exhibited the Joffe effect to a remarkable degree. When immersed in water, crystal rods could be tied into knots within a few seconds (Fig. 19).

[3]It should be noted, however, that this specimen had numerous growth steps and ridges on its surface; these could have acted as stress concentrators and thereby caused premature fracture.

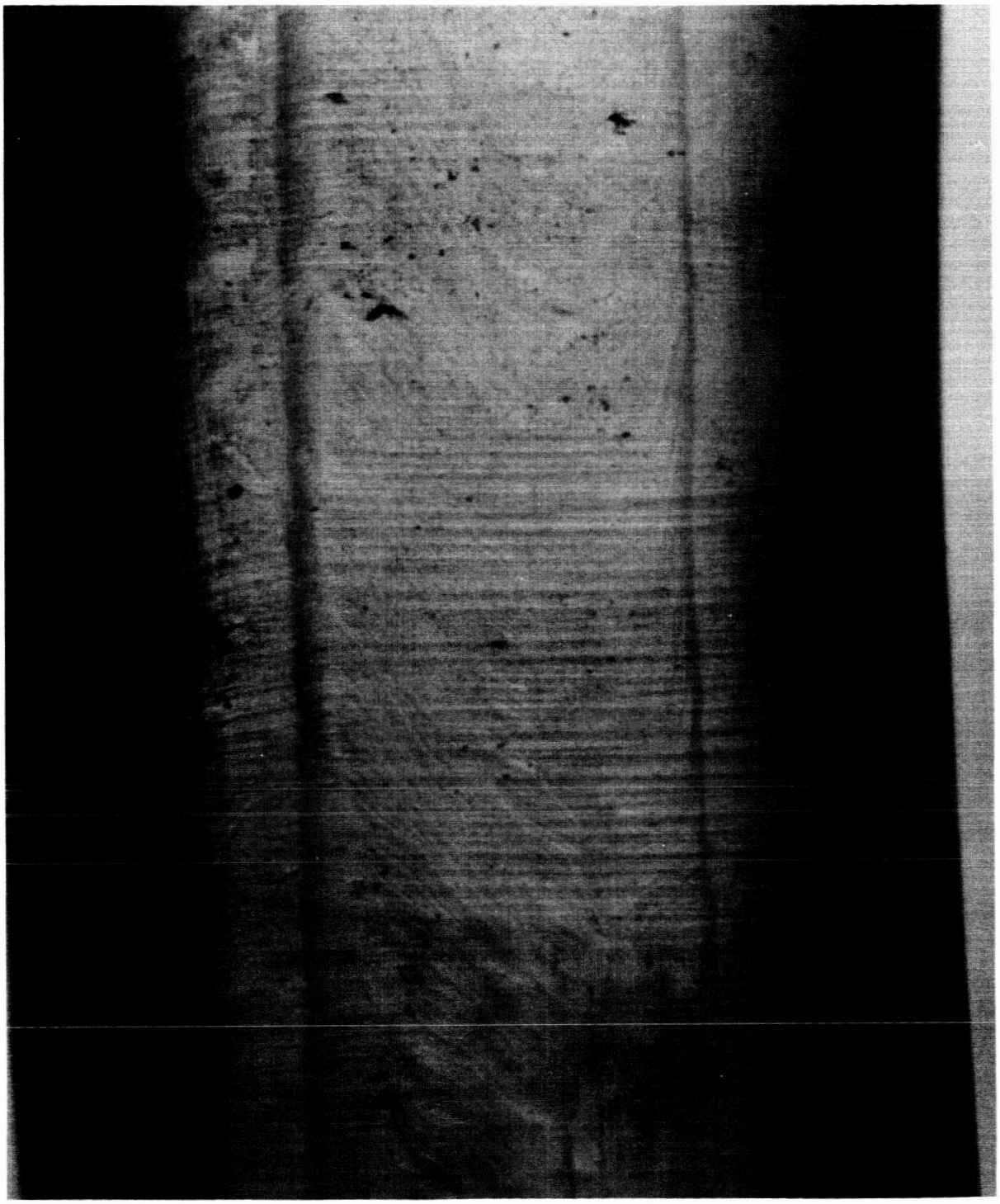

Fig. 18. Slip bands on compressively deformed surface of bent NaCl crystal rod

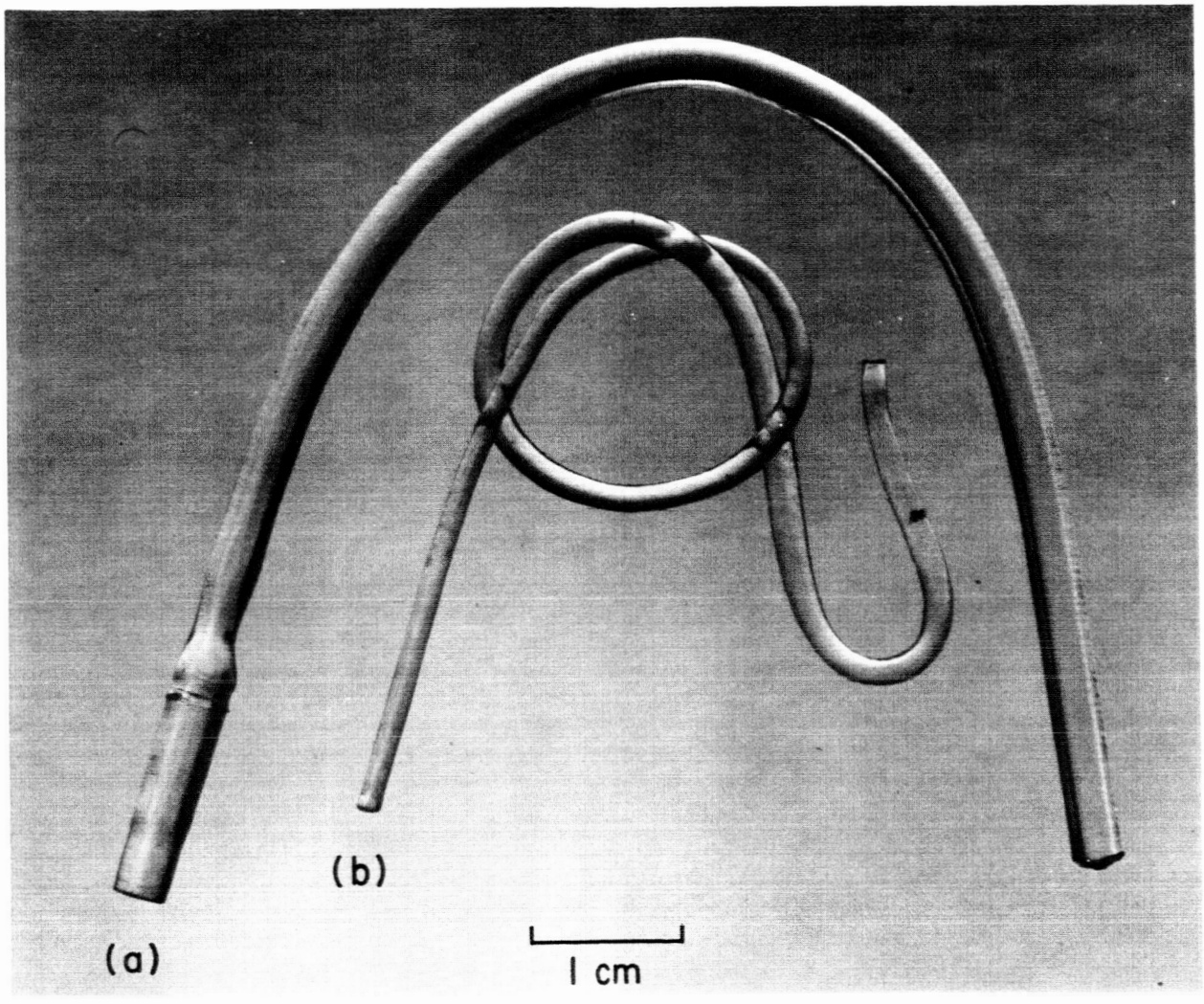

Fig. 19. As-grown NaCl crystals bent (a) in air, and (b) under water

V. DISCUSSION

A. Stress-Strain Idiosyncrasies

Most of the commonly observed stress-strain idiosyncrasies (i.e., initial anelastic regions, soft vs stiff behavior, and other variations in the shape of the curve) are observed in the cleavages and the predeformed crystals but completely absent in the as-grown crystals. Therefore, it appears obvious that these idiosyncrasies are entirely the result of predeformation.

The anelastic foot is observed in approximately half the cases of soft behavior in predeformed crystals and cleavages. It is therefore suggested that this phenomenon is the result of bending the crystal in the direction opposite to that of the predeformational bending, thereby triggering the release of dislocations in the stress fields of pile-ups or bowed-out segments of partially pinned dislocations. At this time, no explanation can be given for the survival of these prestressed areas after annealing.

B. Soft-Stiff Effect

Although the soft-stiff effect is apparently due to predeformation, its exact cause is still obscure. The effect is geometrically specific (i.e., a cleavage is soft when bent in one direction and stiff when bent in the other) even after repeated cycling between the two directions (Refs. 5 and 6); therefore, it cannot be accounted for in terms of a quantitative variation of work hardening by interaction of slip bands with forest dislocations. Another explanation (i.e., the latent hardening of one pair of slip systems by another previously-activated nonorthogonal pair, Refs. 13 and 26) has the requisite geometry but cannot, in its simplest terms, account for the phenomena observed in the tests previously described. In latent hardening experiments on sodium chloride (Ref. 26), the "hard" direction has a much higher flow stress than the soft direction but shows no work hardening; it is the soft direction that, after activation of the hard slip systems, shows a higher work-hardening rate. The explanation of this discrepancy may lie in either the inherent differences between bending and compression tests, or in a more complex latent-hardening interaction between all six slip systems.

In any case, the mechanism of latent hardening is still obscure. One possible cause of latent hardening and stiffening is dislocation-dipole ribbons (or, as they are sometimes called, "debris") formed by the intersection of dislocations during predeformation. This has been used to explain the transition from stage I to stage II deformation (Ref. 25). If we assume a mechanism of this type, it is not difficult to see how the soft-stiff effect could persist through annealing. Dislocations are rearranged during annealing and/or polygonalization, but their concentration and orientation are likely to remain relatively unchanged. For similar reasons, it does not seem likely that dislocation dipoles would be removed easily by annealing. We could therefore expect that the orientation of the soft-stiff effect, as determined from the birefringence patterns of as-cleaved specimens, would persist through annealing. The absence of such a correlation has been reported elsewhere (Ref. 6), but the tests in this Report, although inconclusive, suggest that the expected correlation does exist.

Perhaps the real key to the interpretation of this effect lies in the relative work-hardening rates between the first and second stages of these modes of deformation. It almost seems as if, in the stiff mode, the two stages of deformation had been interchanged. Further study of this phenomenon should be made, not on cleavages, whose predeformation is indeterminable, but on crystal rods subjected to measured amounts of predeformation.

C. Effect of Water Polishing

Presumably, the other, less spectacular variations in the stress-strain curves, such as quasi-parabolic hardening, kinks, and variations in yield stress, are also due to interference between the active slip systems and artifacts of predeformation. There is, however, one such effect that was observed in as-grown crystals, namely, the increase in stage II work hardening by water polishing. There is some possibility that this was caused by slight amounts of predeformation from handling during polishing, but the effect seems too regular for such an explanation. We may reason that the polishing solution (or pyridine rinse) reacted with the crystal surface to produce a barrier to emerging dislocations. It is hard to see, however, why this barrier should have no effect in the first stage of deformation and so marked an effect on the second. Moreover, the usual explanation for the transition to second-stage deformation is the activation of oblique slip systems (Refs. 25 and 26) and it is not obvious that this would be strongly affected by surface effects.

D. Linear Relation Between T_y and G_I

Aside from the absence of stress-strain idiosyncrasies, the most remarkable property of the as-grown crystals is the linear relation between the yield stress and slope of stage I deformation (Eq. 5). Significantly, this equation predicts that a crystal with no initial work hardening would have a resolved shear stress of 18 g/mm²; this is well below 35 g/mm², the minimum value for the resolved shear stress of NaCl as estimated experimentally by Rothwell and Greenler (Ref. 3). Nonetheless, it must be remembered that all of the crystals presented in this Report were similar with respect to starting material, furnace atmosphere, growth rate, cooling rate, and subsequent storage conditions. This uniformity of history may have eliminated parameters which, if varied, could have caused additional variations in mechanical behavior.[4] Hence, Eq. (5) should, at present, be regarded as applying only to the crystals described in this Report.

We may conjecture that the variation in the stress-strain curves of the as-grown crystals is caused by a defect which simultaneously raises the yield stress and the work-hardening rate. The most likely sources of such variation are the dislocation density and the impurity concentration. The density of dislocations does affect the yield stress and the work-hardening rate, but in opposite directions; a low dislocation density causes a pronounced yield drop whereas a high density causes work hardening (Ref. 27). Therefore, this explanation does not seem likely. On the other hand, a divalent ion, such as calcium, is capable of raising both the yield stress and the stage I work-hardening rate (Ref. 28). In accordance with this hypothesis, a comparison was made between the yield stress and the calcium concentration of the as-grown crystals (Fig. 20). Excluding specimen 7-1 (which is also anomalous with respect to Eq. 5), there is, within experimental error, a linear relation between the two parameters

$$G_I \simeq 33.5\,(T_y - 18) \simeq 184C \qquad (6)$$

which predicts a yield stress of 18 g/mm² for a pure crystal. This correlation is indeed encouraging, but it must be pointed out that the analyses (Table 1) are so unreliable as to be nearly worthless. Moreover, nothing

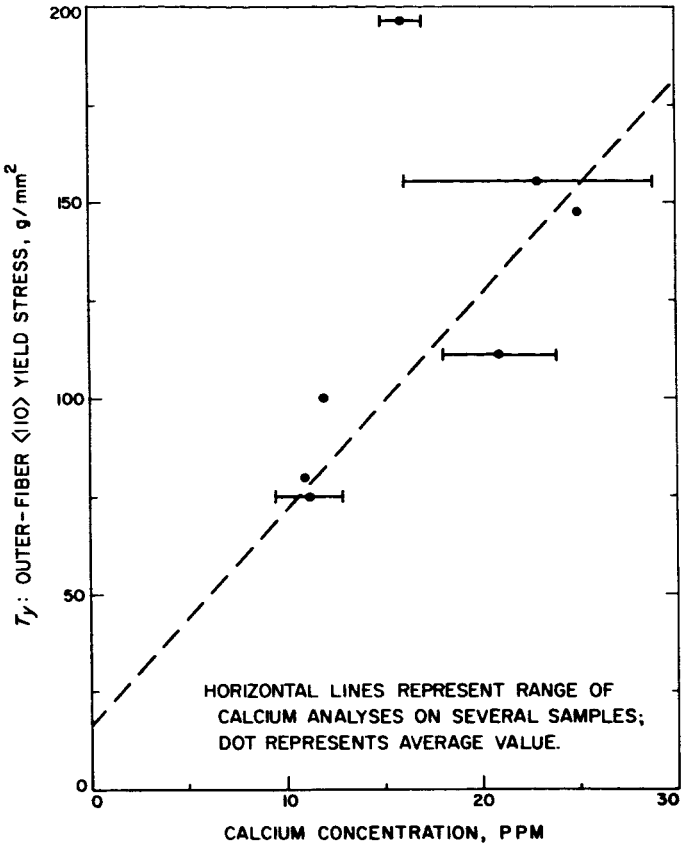

Fig. 20. Yield stress vs calcium concentration in as-grown NaCl crystals (horizontal lines represent range of calcium analysis on several samples; dot represents average value)

is known about the other variable quantities in the crystals such as the anion concentrations, vacancy concentrations, or dislocation densities. Indeed, the calcium concentration may merely imperfectly reflect the variation in some other parameter that more directly affects the mechanical behavior of the crystals. Therefore, this correlation should be regarded merely as an attractive subject for further investigation using high-purity crystal rods.

E. Atmospheric Embrittlement

The controversial subject of atmospheric embrittlement (Refs. 7 through 11) was not directly studied in the experiments reported herein. However, the qualitative observation has been made that, whereas the as-grown crystals retain their ductility even after prolonged exposure to varying atmospheric conditions, deformed crystals rapidly become brittle. It therefore seems possible that atmospheric embrittlement is caused by the preferential

[4]For example, divalent ions present as individual substitutional defects tend to raise the flow stress (Ref. 28). The same impurity present as dislocation-decorating precipitates would be more likely to raise the yield point and/or the work-hardening rate. Therefore, variations in heat treatment prior to testing would affect the partition of the impurities between solution and precipitates and thereby affects the mechanical properties.

reaction of atmospheric components with surface artifacts of deformation, such as slip bands or dislocation dipoles. This hypothesis also appears to be worthy of further study.

F. Joffe Effect

The remarkable enhancement of the plasticity of as-grown crystals when deformed under water is especially significant. Most previous explanations of the Joffe effect have assumed that the water in which the crystal was immersed served merely to dissolve antecedent causes of embrittlement such as microcracks (Ref. 29), precipitates (Ref. 12), growth steps (Ref. 11), or adsorbed gases (Ref. 4). According to these theories, a crystal bent under water should have no greater ductility than a carefully water-polished crystal.

The present work shows that as-grown crystals, lacking these surface defects and possessing a high degree of intrinsic ductility that is not so much enhanced as impaired by water polishing, exhibit greatly enhanced ductility. One explanation for this "dynamic Joffe effect" is that the heat of hydration substantially diminishes the energy required to create new surface at emerging slip bands. Another explanation, proposed by Mendelson (Ref. 30), is the dissolution of subsurface barriers to slip (i.e., dislocation pile-ups and cross-slipped screw dislocations). This mechanism is analogous to the enhancement of ductility in metals by electropolishing during deformation. It is also possible, however, to explain the Joffe effect as a ramification of the thermodynamic fact that a crystal becomes more soluble under stress (Refs. 31 and 32). This phenomenon has been experimentally confirmed for sodium chloride by the observations that the solubility of salt crystals was increased during plastic deformation (Ref. 33). It has also been noted at this laboratory that, when salt crystals were subjected to bend tests under water, the stress enhancement of solubility was so great that it caused preferential dissolution at the load members, thereby forming notches. Moreover, an examination of the knotted crystal (Fig. 19) shows preferential thinning in the region of the sharpest bends. According to this theory, any surface stress concentrations that might cause premature fracture would be preferentially dissolved before they could do any harm. This theory in no way excludes Mendelson's and both mechanisms are probably operative in the dynamic Joffe effect.

VI. CONCLUSION

It has been demonstrated that most of the inconsistencies in the existing literature on the mechanical properties of sodium chloride crystals are the result of artifacts, introduced during cleavage, which are not removed by conventional annealing and polishing techniques. In contrast, as-grown crystals deform in a relatively simple and comprehensible manner and exhibit properties, such as the dynamic Joffe effect and the absence of atmospheric embrittlement, which have not hitherto been reported. Therefore, only as-grown crystals, of the highest possible purity and perfection, should be used in future research on the subject.

NOMENCLATURE

Symbols

a horizontal distance between outer and inner load members; $\equiv$ 10 mm at beginning of test [mm]

D deflection of inner load members; assumed to be equivalent to cross-head deflection [mm]

E outer-fiber tensile strain, as calculated on the assumption of pure elastic bending [dimensionless]

E_f outer-fiber tensile strain at termination of test (i.e., at fracture or >90-deg bend) as calculated from the cross-head load and deflection

E_f' outer-fiber tensile strain at termination of test as calculated from measured bend radius and thickness of specimen

E_y outer-fiber tensile strain at yield point

G_I integrated work-hardening rate; i.e., average slope of stress-strain curve, dT/dE, during the first stage of plastic deformation [g/mm²]

h distance from center line of crystal cross section (i.e., centroid of cross-section moment of inertia) to bottom crystal surface [mm]

I cross-section moment of inertia; $\int_{-h}^{h} wx^2\,dx$ of crystal cross section. The center line is so chosen that the moment of inertia of the top and bottom halves are equal [mm⁴]

K slope of G_I vs T_y for as-grown crystals; $G_I/(T_y - 18)$ [dimensionless]

L total load on specimen; assumed equal to cross-head load and assumed to be equally divided between the two inner load members [g]

M bending moment about crystal at any given point [g • mm]

R radius of bending of center axis of crystal at termination of test [mm]

S tensile stress on outer fiber of crystal, as calculated on the assumption of pure elastic bending [g/mm²]

T resolved $<110>$ $\{1\bar{1}0\}$ shear stress on outer fiber, as calculated on the assumption of pure elastic bending; $\equiv S/2$ [g/mm²]

T_y resolved $<110>$ $\{1\bar{1}0\}$ shear stress on outer fiber at yield point [g/mm²]

w width of crystal at any given point; for calculation of width-to-thickness ratio, $w/2h$, w is measured at centroid [mm]

Y Young's modulus [g/mm²]

y yield point of outer fiber; measured herein as first noticeable deviation from linear elastic behavior (excluding anelastic feet at beginning of test)

Φ angle between normal of slip plane and axis of tension; 45 deg for NaCl

λ angle between slip direction and axis of tension; 45 deg for NaCl

REFERENCES

1. Pratt, P. L., "Similar Glide Processes in Ionic and Metallic Crystals," *Acta Metallurgica*, Vol. 1, 1953, pp. 103–104.

2. Stearns, C. A., Pack, A. E., and Lad, R. A., "Factors Affecting the Ductility and Strength of NaCl Single Crystals Tested in Flexure," *Journal of Applied Physics*, Vol. 30, 1960, pp. 231–234.

3. Rothwell, W. S., and Greenler, R. G., "Annealing and Yield Stress of NaCl Single Crystals," *Journal of American Ceramics Society*, Vol. 47, 1964, pp. 585–587.

4. Aerts, E., and Dekeyser, W., "Gases in Rocksalt and the Joffe Effect," *Acta Metallurgica*, Vol. 4, 1956, pp. 557–558.

5. Greenler, R. G., and Rothwell, W. S., "Ductility of NaCl Crystals," *Journal of Applied Physics*, Vol. 31, 1960, pp. 616–617.

6. Rothwell, W. S., and Greenler, R. G., "Mechanical Behavior of Sodium Chloride Crystals in Flexure," *Journal of American Ceramics Society*, Vol. 45, 1962, pp. 607–610.

7. Lad, R. A., Stearns, C. A., and Del Duca, M. G., "Factors Affecting the Plasticity of Ionic Crystals," *Acta Metallurgica*, Vol. 6, 1958, pp. 610–611.

8. Parker, E. R., et al., *The Mechanical Properties of Some Ionic Materials, and the Effect of Surface Conditions on Their Room Temperature Ductility*, First Technical Report, Contract No. AF49(638)-56, November, 1957.

9. Machlin, E. S., and Murray, G. T., "Effect of Atmosphere Conditions on the Brittleness of NaCl," *Journal of Applied Physics*, Vol. 30, 1959, pp. 1731–1732.

10. Otterson, D. A., "Influence of Room-Temperature Atmospheric Reaction Products on the Ductility of Sodium Chloride Single Crystals," *Journal of Chemical Physics*, Vol. 38, 1963, pp. 1481–1486.

11. March, D. M., "Stress Concentrations at Crystal Surfaces and the Embrittlement of Sodium Chloride," *Philosophical Magazine*, Vol. 5, 1960, pp. 1197–1199.

12. Stokes, R. J., Johnston, T. L., and Li, C. H., "Environmental Effects on the Mechanical Properties of Ionic Solids with Particular Reference to the Joffe Effect," *Transactions of the Metallurgical Society of the AIME*, Vol. 218, 1960, pp. 655–662.

13. Alden, T. H., "Extreme Latent Hardening in Compressed Lithium Fluoride Crystals," *Acta Metallurgica*, Vol. 11, 1963, pp. 1103–1105.

14. Gilman, J. J., "Nucleation of Dislocation Loops by Cracks in Crystals," *Journal of Metals*, Vol. 9, 1957, pp. 449–454.

15. Shlichta, P. J., "Orientation Effects in Sodium Chloride Crystals," *JPL Research Summary No. 36-10, Vol. I*, 1961, pp. 76–78, and "Morphology of Sodium Chloride Crystals," *JPL Space Programs Summary No. 37-15, Vol. IV*, 1962, pp. 88–91, Jet Propulsion Laboratory, Pasadena, California.

REFERENCES (Cont'd)

16. Johnson, C. R., "Hydrolysis of Alkali Chlorides," *Journal of Physical Chemistry*, Vol. 39, 1935, pp. 791–795.

17. Otterson, D. A., "On the Presence of NaOH in Crystalline NaCl," *Journal of Chemical Physics*, Vol. 33, 1960, pp. 227–229.

18. Mendelson, S., "Dislocation Etch-Pit Formation in Sodium Chloride," *Journal of Applied Physics*, Vol. 32, 1961, pp. 1579–1583.

19. Shlichta, P. J., and Cremer, H., *Semiautomatic Counter for Dislocation Etch Pits and Other Point Arrays*, Jet Propulsion Laboratory, Pasadena, California (to be published).

20. Belt, R. F., "Crystal Perfection of Sodium Chloride Grown by the Stockbarger Technique" (to be published).

21. Timoshenko, S., and MacCullough, G. H., *Elements of Strength of Materials*, D. Van Nostrand Co., New York, 1940, pp. 113–116, 2nd ed.

22. *Steel Construction*, American Institute of Steel Construction, 1937, p. 345, 3rd ed.

23. Cottrell, A. H., *Dislocations and Plastic Flow in Crystals*, Clarendon Press, Oxford, 1953, p. 5.

24. Stokes, R. J., Johnson, T. L., and Li, C. H., *Kinking and the Fracture of Ionic Solids*, Twelfth Technical Report, Office of Naval Research Project Nonr-2456(00)NR-032-451, June, 1961.

25. Davidge, R. W., and Pratt, P. L., "Plastic Deformation and Work Hardening in NaCl," *Physica Status Solidi*, Vol. 6, 1964, pp. 759–776.

26. Alden, T. H., "Latent Hardening and the Role of Oblique Slip in the Strain Hardening of Rock-Salt Structure Crystals," *Transactions of the Metallurgical Society of the AIME*, Vol. 230, 1964, pp. 649–656.

27. Johnston, W. G., "Yield Points and Delay Times in Single Crystals," *Journal of Applied Physics*, Vol. 33, 1962, pp. 2716–2730.

28. Brown, L. M., and Pratt, P. L., "Strain Aging in $CdCl_2$-doped Rock Salt," *Philosophical Magazine*, Vol. 8, 1963, pp. 717–734.

29. Joffe, A., *The Physics of Crystals*, McGraw-Hill Book Co., New York, 1928.

30. Mendelson, S., "Dislocations and Plastic Flow in NaCl Single Crystals: I and II," *Journal of Applied Physics*, Vol. 33, 1962, pp. 2175–2186.

31. Riecke, E., "Ueber die Züstandsgleichung von Clausius," *Nachrichter Königlichten von der Gesellschaft der Wissenschaften zer Gottingen, Mathematisch-physikalische Klasse*, 1894, pp. 285–290.

32. Conens, C. W., "Growth and Dissolution of Crystals under Linear Pressure," *Crystal Growth: Discussions of the Faraday Society*, Vol. 5, Butterworth's Scientific Publications, London, 1959, pp. 267–271.

33. Guylai, F., "Neuer Beträge zur Physik der Kristal," *Academiae Scientiarum Hungaricae*, Vol. 5, 1956, pp. 425–443.

ACKNOWLEDGMENT

The author wishes to thank William Stout, whose skill and patience in growing and testing these crystals made this work possible. Grateful acknowledgment is also made to Michael Reischel for assistance in testing; to John Adkins for dislocation etching and photomicrography; to King Titus for data reduction; and to L. D. Jaffe, Howard Martens, and C. E. Levoe for their guidance and consultation.

A special debt of gratitude is owed to the late Professor Spiro Kyropoulos, who first developed the technique of crystal pulling and who taught the author the subtleties of this art.